# SEA SURFACE KINETIC ENERGY AS A PROXY FOR MESOSCALE LIGHT LIMITATION FOR PHYOPLANKTON IN THE SOUTHERN OCEAN

by

Joseph Christopher Gradone

A thesis submitted to the Faculty of the University of Delaware in partial fulfillment of the requirements for the degree of Master of Science in Marine Studies

Fall 2018

**SEA SURFACE KINETIC ENERGY AS A PROXY FOR MESOSCALE LIGHT LIMTATION FOR PHYTOPLANKTON IN THE SOUTHERN OCEAN**

by

Joseph Christopher Gradone

Approved: _____
Matthew J. Oliver, Ph.D.
Professor in charge of thesis on behalf of the Advisory Committee

Approved: _____
Mark A. Moline, Ph.D.
Director of the School of Marine Science and Policy

Approved: _____
Estella A. Atekwana, Ph.D.
Dean of the College of Earth, Ocean, and Environment

Approved: _____
Douglas J. Doren, Ph.D.
Interim Vice Provost of the Office of Graduate and Professional Education

**ACKNOWLEDGMENTS**

I would like to thank and acknowledge my advisor, Dr. Matthew Oliver, for giving me the opportunity to pursue my Masters and providing me with both academic and personal guidance. Matt, thank you for pushing me as a scientist and for always encouraging the lab the think critically. I would like to thank my advisory committee Dr. Carlos Moffat, University of Delaware, Dr. Andrew Irwin, Mount Allison University, and Dr. Tobias Kukulka, University of Delaware, for their guidance through this Master's project. I would like to acknowledge my lab mates, Dr. Danielle Haulsee, Dr. Matthew Breece, Cordielyn Goodrich, and Katie Hudson for their constant support and guidance as well as making my graduate experience unforgettable. I would also like to thank Alex Davies, United States Naval Academy, for his guidance and for his Master's work with Dr. Oliver which was truly the foundation for my research project.

Last but not least, I would like to thank my family. Thank you, Sarah, for your unwavering love and support, especially during the past two years. Thank you to my family who have always encouraged me to pursue my goals at every stage of my life. Without them, I would not be where I am today.

## TABLE OF CONTENTS

## LIST OF TABLES

## LIST OF FIGURES

## ABSTRACT

The Southern Ocean is classified as a high nutrient, low chlorophyll region as surface waters are typically macro-nutrient (e.g. nitrogen and phosphorous) rich in the austral summer, yet they are characterized by patchy, intense phytoplankton blooms within a generally unproductive environment. The mechanisms controlling phytoplankton abundance include turbulent mixing, available light, respiration and predation rates, and nutrient availability. While there is much debate about the *initiation* of phytoplankton blooms in the Southern Ocean, there is also significant variation in phytoplankton bloom dynamics *within* a growing season, suggesting many different mechanisms are contributing to patchy phytoplankton distributions.

Using data from 2003 to 2017, a surprising relationship between *in situ* and satellite-derived chlorophyll and modelled kinetic energy was observed. High chlorophyll concentrations were not observed in either remotely sensed or *in situ* data while kinetic energy was high throughout the entire Southern Ocean. Consequently, low kinetic energy appears to be a necessary, but not sufficient, precondition for phytoplankton blooms throughout the Southern Ocean. In December, surface phytoplankton concentration appears to decrease due to high kinetic energy simply diluting their concentration in the water column. However, in January and February high kinetic energy appears to limit phytoplankton abundance through a mesoscale light limitation by decreasing the time they spend in the euphotic zone. Analysis of this relationship through a time dependent, probabilistic model, combined with in-situ observations of water column structure show that high kinetic energy deepens the mixed layer through turbulent mixing, potentially limiting the availability of light.

These probabilistic models suggest that the spatial pattern in kinetic energy in the Southern Ocean explains up to 30% of the variability in the distribution of chlorophyll concentration. These findings indicate that KE is a significant factor in structuring the spatial distribution in Southern Ocean chlorophyll.

# Chapter 1

# INTRODUCTION

## 1.1 Background and Motivation

In well lit, nutrient rich regions of the surface ocean, phytoplankton drawdown atmospheric carbon dioxide ($CO_2$) by converting it into organic matter via oxygenic photosynthesis. Photosynthesis is an oxidation-reduction reaction that can be written in a general form:

$$CO_2 + 2H_2O + Light \xrightarrow{chlorophyll-a} CH_2O + H_2O + O_2$$

During photosynthesis, light energy is converted into chemical bond energy to form organic compounds. In this reaction, chlorophyll-*a* is a photosynthetic pigment used to absorb light energy, acting as an electron catalyst in the reduction half of the photosynthetic reaction (Falkowski & Raven, 2007). When phytoplankton biomass is not consumed by other trophic levels, they senesce and sink into the deep ocean, transporting carbon from the surface ocean to the deep sea. Globally, the biological pump transfers about 10 Pg ($1x10^{13}$ kg) of carbon per year from the atmosphere to the deep ocean (Bopp et al., 2005). Once in the deep ocean, phytoplankton biomass can either be decomposed by microbes and converted back into dissolved inorganic $CO_2$ or buried in sediments on a timescale of millions of years (Ciais, 2013). Because of phytoplankton and their role in the biological pump, the ocean plays a major part in the global carbon cycle. The ocean is the largest reservoir of carbon and has sequestered approximately 48% of anthropogenic atmospheric $CO_2$ during the period of 1800 to 1994 (Falkowski et al., 2000; Sabine et al., 2004, IPCC, 2013).

The primary mechanisms that cause phytoplankton to bloom are varied. Phytoplankton blooms are affected by factors such as turbulent mixing, available light, respiration and predation rates, and nutrient availability. While different explanations acknowledge that a combination of these features are significant for bloom development, they differ in what is considered the primary mechanism. An important early insight into this process was provided through the critical depth hypothesis, formalized by Sverdrup in 1953, which proposes that phytoplankton blooms occur when the mixed layer depth shoals above a critical depth, keeping phytoplankton cells in areas of higher light where phytoplankton growth exceeds loss. The critical depth hypothesis essentially attributes blooms to enhanced growth rates in response to improved light conditions (Sverdrup, 1953). Huisman et al.'s (1999) critical turbulence hypothesis nuances this result by suggesting that near surface turbulence, not the mixed layer, is responsible for keeping phytoplankton in high light conditions. The critical turbulence hypothesis applies when there is a relaxation of turbulent mixing in waters of low background mixing, regardless of the thickness of the upper water column (Huisman et al., 1999). In contrast to light mechanisms determining the formation of phytoplankton blooms, Behrenfeld's dilution-recoupling hypothesis notes that blooms often occur while the mixed layer is deepening, not shoaling. Behrenfeld proposes that deepening mixed layers reduce phytoplankton-grazer interaction, thus increasing phytoplankton growth rates (Behrenfeld, 2010).

The Southern Ocean (SO) is classified as a high nutrient, low chlorophyll (HNLC) region as surface waters are typically macro-nutrient (e.g. nitrogen and phosphorous) rich in the austral summer, yet they are characterized by patchy, intense phytoplankton blooms within a generally unproductive environment (Arrigo et al.,

2008; Moore & Abbott, 2000). Furthermore, because the SO is a high latitude ecosystem, it is seasonally light limited (El-Sayed, 1987). Increases in phytoplankton productivity in the SO are generally linked to increases in a deficient micronutrient, iron (Martin, 1990). Iron concentration is known to increase either locally due to aeolian deposition (i.e. dust storms) or over larger regions of the Southern Ocean via upwelling (Boyd et al., 2007). Because iron is the limiting nutrient for phytoplankton blooms, SO waters have been the focus of several artificial iron enrichment experiments (Boyd et al., 2000; Coale et al., 2004; Gervais at al., 2002; Hoffmann et al., 2006, Smetacek et al., 2012). However, despite the number of studies pertaining to iron and phytoplankton abundance, it appears that the availability of light, mediated by changes in the mixed layer depth, is still the major driver for phytoplankton blooms (de Baar et al., 2005). While iron and light are both important limiting factors for SO blooms, the mechanisms controlling mesoscale phytoplankton abundance and the biological pump in the SO remain largely unresolved.

While there is much debate about the *initiation* of phytoplankton blooms in the SO, there is also significant variation in phytoplankton dynamics *within* a growing season, suggesting many different mechanisms are contributing to phytoplankton dynamics. One of the most curious proxies for phytoplankton concentration within the growing season was described by Davies in a 2015 study in the Drake Passage region of the Southern Ocean. Davies (2015) showed that high chlorophyll values were not coincident with high surface kinetic energy (KE) in both satellite and biofloat observations (Figure 1.1). Davies proposed that kinetic energy may have an overarching control on phytoplankton because of its potential to deepen the mixed layer, thus limiting phytoplankton's exposure to light. Davies found that, on average,

when higher kinetic energy leads to increased mixing and deeper mixed layer depths (Figure 1.2). In contrast, when KE is low, the mixed layer shoals, potentially alleviating the light limitation on phytoplankton (Davies, 2015).

This study focuses on phytoplankton bloom dynamics *within* the summer growing season by examining this unique and unexpected relationship between KE and chlorophyll. First, the analysis conducted in the Drake Passage region is expanded to the entire Southern Ocean. Next, a predictive model was built to understand the processes related to this KE-chlorophyll relationship. Finally, *in situ* floats were used as validators and compared satellite and modeled observations with a monthly mixed layer depth climatology to better understand the mechanisms behind this relationship.

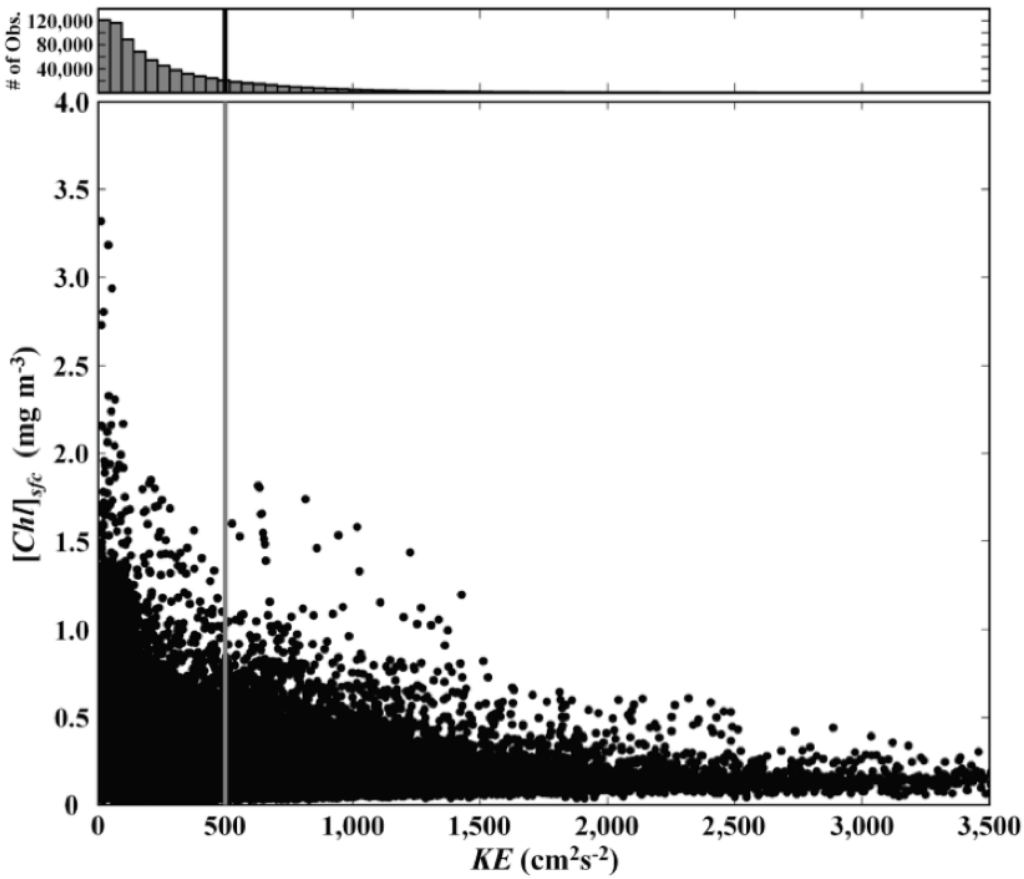


Figure 1.1: MODIS *Aqua* five-day composite surface chlorophyll-*a* concentration plotted with coincident estimates of KE specifically in the Drake Passage region of the Southern Ocean. Figure from Davies (2015).

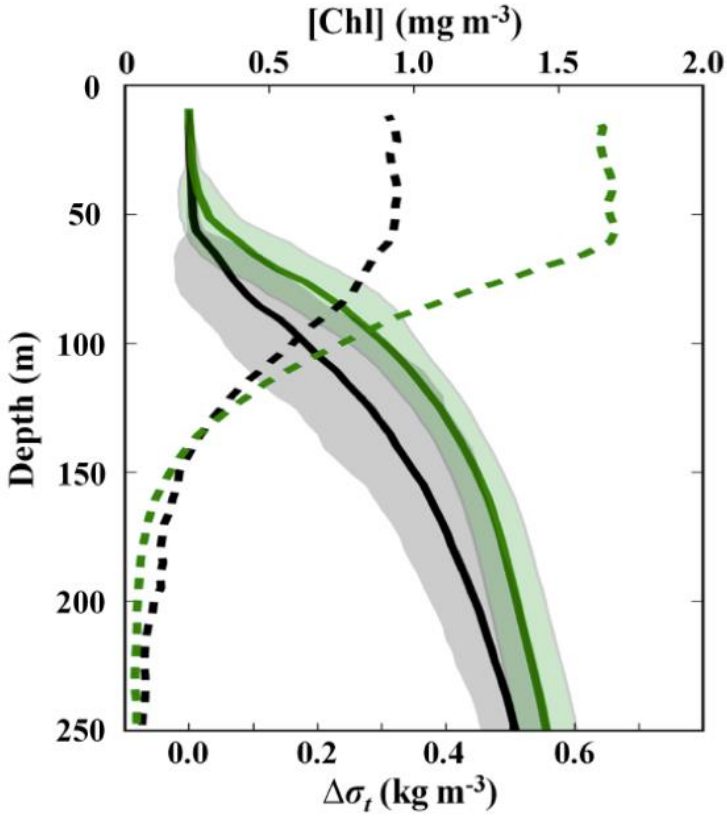


Figure 1.2: Mean normalized density profiles ($\Delta\sigma_t$) from the biofloat (solid lines) plus one standard deviation (shading) for high (black) and low (green) levels of surface mesoscale kinetic energy per unit mass (KE) calculated at biofloat locations. The dashed lines denote the mean chlorophyll-*a* profiles for high (black) and low (green) levels of KE. 500 $cm^2$ $s^{-2}$ is the transition between high and low KE. $\sigma_t$ is the density calculated from only biofloat temperature and salinity profiles minus 1,000. $\Delta\sigma_t$ is the $\sigma_t$ value at each depth normalized by the surface $\sigma_t$ value. Figure from Davies, 2015.

# Chapter 2

# METHODS AND MATERIALS

## 2.1 Southern Ocean Satellite Chlorophyll-*a*

Estimates of Southern Ocean surface chlorophyll (CHL) concentrations and distributions were made using the National Aeronautics and Space Administration's (NASA) Moderate Resolution Imaging Spectroradiometer (MODIS *Aqua*). This satellite has a 705 km, sun-synchronous, near polar orbit (Pagano & Durham, 1993). Standard NASA processing flags were used to remove data in the Southern Ocean for a failure in atmospheric or aerosol corrections, cloud or ice contamination, and high solar zenith (Esaias et al., 1998).

However, NASA's OC3M surface chlorophyll algorithm for the MODIS *Aqua* satellite significantly underestimates chlorophyll concentrations at high latitudes (Dierssen & Smith, 2000; Cota et al., 2003; Gregg & Casey, 2004; Kahru & Mitchell, 1999; Strutton et al., 2011). To correct for this, a Southern Ocean specific chlorophyll algorithm was used which greatly improved upon the standard MODIS algorithm (Johnson et al., 2013). This new algorithm is:

1) $$Chl = 10^{\left(0.6994 - 2.0384R_{MA} - 0.4656R_{MA}^{2} + 0.4337R_{MA}^{3}\right)}$$

2) $$R_{MA} = log10\left(Rrs_{\left(\frac{443}{555}\right)} > Rrs_{\left(\frac{490}{555}\right)}\right)$$

where Rrs is remote sensing reflectance ($sr^{-1}$) and the log10 argument in $R_{MA}$ indicates that the algorithm uses the maximum of the two ratios (Johnson et al., 2013). Using this new algorithm, the dynamic range of detection increased by 138% and underestimation of Southern Ocean chlorophyll was reduced (Johnson et al., 2013).

Five day composites of surface chlorophyll-*a* concentration using the Johnson et al. (2013) algorithm were made from daily, 9-km resolution, level-3 remote sensing

reflectance data. The focus of this research is on chlorophyll concentrations in the open ocean. Therefore, spatial masks were applied to eliminate the effect that islands and shallow coastal waters may have on surface chlorophyll concentrations (Figure 2.1).

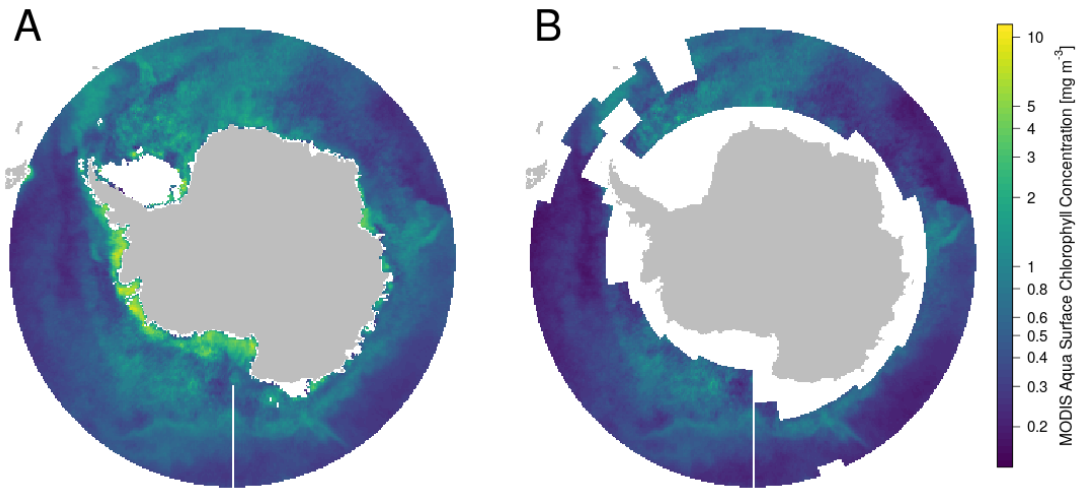


Figure 2.1: (A) Unmasked averaged MODIS *Aqua* surface chlorophyll concentration from 2003-2017. (B) Masked averaged MODIS *Aqua* surface chlorophyll concentration from 2003-2017.

## 2.2 Mesoscale Kinetic Energy

Mesoscale kinetic energy estimates are derived from the National Oceanic and Atmospheric Administration's (NOAA) unfiltered, 1/3° resolution, five day-averaged Ocean Surface Current Analysis-Real time (OSCAR currents) data product (https://podaac.jpl.nasa.gov/dataset/OSCAR_L4_OC_third-deg). OSCAR surface currents are computed by combining a quasi-steady geostrophic model with wind-driven ageostrophic currents and thermal wind adjustments (Bonjean & Lagerloef,

2002). These currents are representations of averaged flow over the upper 30 m of the ocean and are calculated by:

$$3)\quad if\bar{U} = -g\nabla\varsigma + \frac{h}{2}\nabla\theta + \frac{\tau - AU'(-h)}{h}$$

In this equation, U(x,y,z,t) ≡ u + iv is the horizontal velocity vector where the overbar denotes an averaged velocity to a depth h (30 meters). U' ≡ $U_z$ denotes the vertical shear which is assumed to be equal to τ/A at the surface of the ocean and equal to zero at a depth > h = 30 m (Bonjean & Lagerloef, 2002). ∇ ≡ ∂/∂x + i∂/∂y where the vector wind stress field divided by the characteristic density is represented by $\tau = \tau^x + i\tau^y$ (Bonjean & Lagerloef, 2002). g is the gravitational constant, ζ is the displacement of the ocean-atmosphere interface, θ is the buoyancy force proportional to ∇(Sea Surface Temperature), *f* is the coriolis force, and A is the depth-uniform eddy viscosity that characterizes turbulent vertical mixing (Bonjean & Lagerloef, 2002). The first term on the right-hand side of this equation, -g∇ς, represents the pressure gradient force (geostrophy) which is adjusted by the contribution of the second term, (h/2)∇θ, which is the buoyancy gradient. The last term on the right-hand side of the equation represents the net drag force applied by the wind stress to a depth h.

OSCAR uses a variational analysis of Special Sensor Microwave Imager (SSM/I) winds by Atlas et al. (1996) to compute surface winds with the wind stress vectors being computed using the drag relationship used by Large & Pond (1981). OSCAR also incorporates Jason-1 and Envisat altimetry data. The data is packaged as discrete, temporal blocks of five-day averaged currents, from which discrete kinetic energy per unit mas (KE) estimates are obtained,

$$KE = \frac{1}{2}(u^2 + v^2),$$

where u and v are the meridional and zonal components of the OSCAR currents, respectively. With a one-third degree spatial resolution and a five-day sampling period, the OSCAR currents are well-suited to resolve the mesoscale dynamics in the SO which occur on the order of 100 km spatially and 10 days temporally (Daniault & Menard, 1985). Part of the reason it is interesting to compare the relationship that modeled mesoscale surface kinetic energy has with satellite derived chlorophyll concentration is because of the differences in coverage between the two products (Figure 2.2). Because these modeled surface currents are not hampered by clouds, understanding the impact KE has on phytoplankton abundance may provide insight into better estimating the total SO biomass. For spatially coincident satellite estimates of CHL and KE in the SO, the CHL product was linearly interpolated onto the OSCAR 1/3° x 1/3° grid and restricted to South of 55° S.

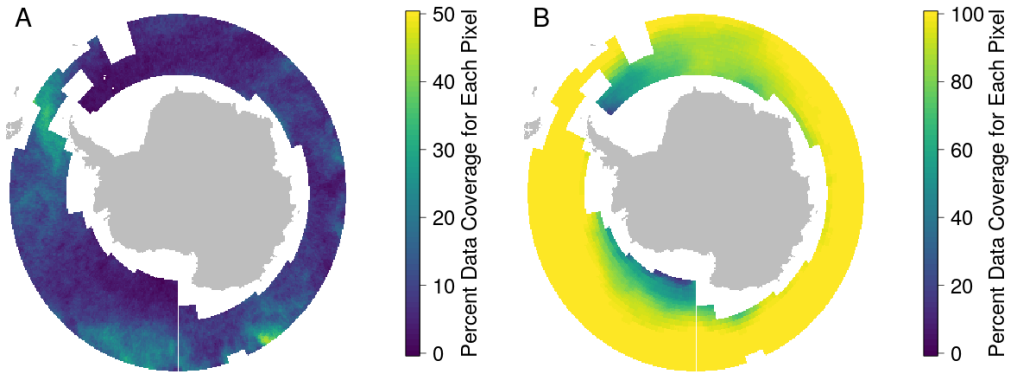


Figure 2.2: (A) Percent of MODIS *Aqua* pixels with surface chlorophyll estimates for 5 day composites from 2003-2017. (B) Percent of OSCAR pixels with surface current estimates for 5 day composites from 2003-2017.

## 2.3 Argo Float Mixed Layer Depth Climatology

While there are several global mixed layer depth products available, there are large uncertainties in the Southern Ocean component of these products (Dong et al., 2008). Dong et al. (2008) used over 42,000 Argo float profiles of temperature, salinity, and pressure from July 2001 to September 2006 in the Southern Ocean (30°S-65°S, 0°E-360°E) to create a MLD climatology. This monthly climatology is objectively mapped onto a 1° x 1° grid. Dong et al. (2008) deemed the mixed layer depth definition that used a potential density difference from the surface (0-20m) of 0.03 kg $m^{-3}$ the most robust for the Southern Ocean.

For use in this study, a time-weighted mean of this monthly climatology was created and matched to the corresponding days of the month containing the five-day averaged OSCAR currents and MODIS CHL observations. For spatially coincident estimates of CHL, KE, and MLD in the SO, MLD products were linearly interpolated onto the OSCAR 1/3° x 1/3° grid and restricted to South of 55° S.

## 2.4 SOCCOM Floats

The Southern Ocean Carbon and Climate Observations and Modeling (SOCCOM) program has deployed biogeochemical sensors on profiling floats in the Southern Ocean since 2014. This program is focused on the Southern Ocean's impact on the anthropogenic carbon budget, ocean biogeochemistry, and climate change (Russell et al., 2014). In addition to the temperature, salinity, and pressure sensors found on traditional Argo floats, these floats carry oxygen, nitrate, pH, chlorophyll fluorescence, and optical backscatter sensors (Johnson et al., 2017). These floats collect data by profiling the water column from their maximum depth, between 1,400 and 2,000 m, before returning to the surface every 10 days (Johnson et al., 2017). Measurements are only made during ascents and are transmitted via the Iridium satellite network after surfacing (Figure 2.3). Sampling resolution is highest in the upper 100 m, less than 1.5 m resolution, but is increasing coarser at greater depths. The sampling resolution of these floats allows for comparison with the other data products used in this study. Table 2.1 summarizes the different data products and their respective spatial and temporal resolution.

Table 2.1: A summary of the different data products used in this study and their spatial and temporal resolution.

| Data Product | Temporal Resolution | Spatial Resolution | Data Provider |
|---|---|---|---|
| **OSCAR Surface Currents** | 5 Days | 1/3° x 1/3° | NOAA |
| **MODIS Chlorophyll-a** | 5 Days | 9 km | NASA |
| **Mixed Layer Depth Climatology** | 5 Days | 1° x 1° | Dong et al. 2008 |

| | | | |
|---|---|---|---|
| **SOCCOM Bio-Floats** | 10 Days | < 1.5 m vertically | SOCCOM |

There are 76 floats (~3,400 profiles) with quality-controlled and adjusted data that have been in the water for at least six months in the SOCCOM database. After removing floats that do not have working chlorophyll sensors (10 floats), applying the land and island masks (535 profiles), and removing the non-summer profiles (2575 profiles), 266 profiles from 31 different floats over 4 years were left to be used in this study.

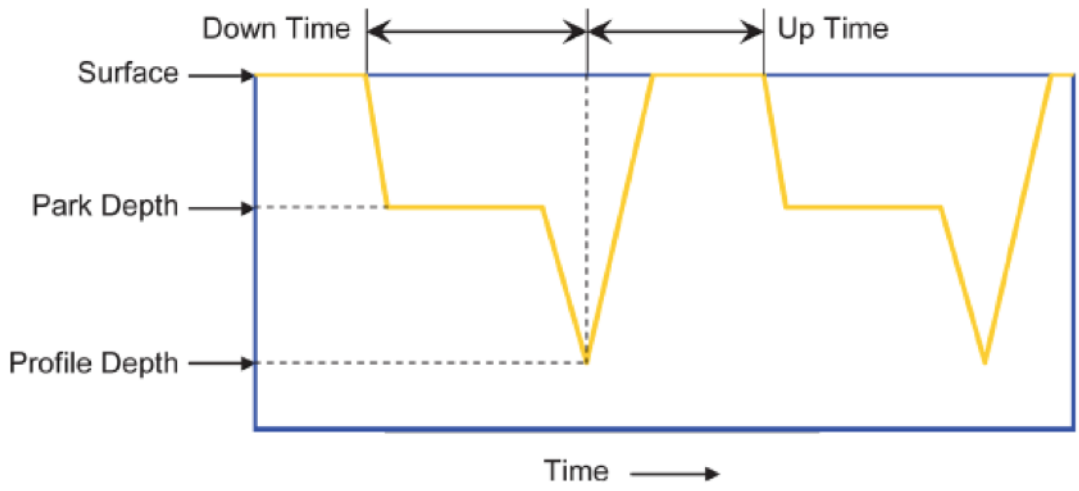


Figure 2.3: APEX float sampling cycle. This is the sampling cycle used by the SOCCOM floats where the total time cycle time (down-time and up-time) is approximately 10 days. The park depth is 1,000 dbar and the profile depth is between 1,400 and 2,000 dbar. From Webb Research (2012).

SOCCOM floats are equipped with one of two types of WET Labs fluorometers, either an ECO-FLBB AP2 with a chlorophyll-*a* fluorometer (Excitation/Emission 470/695 nm) or a MCOMS with the same specifications

(Johnson et al., 2017). Chlorophyll-*a* concentration is estimated according to a WET Labs linear calibration slope of the fluorescence signal (Johnson et al., 2017). Because these raw chlorophyll concentrations suffer from nonphotochemical quenching (NPQ) in the surface ocean and variations in the relationship between chlorophyll fluorescence and chlorophyll concentration due to changes in phytoplankton physiology, SOCCOM performs two important corrections to the raw chlorophyll fluorescence data (Johnson et al., 2017). First, if the sun elevation was greater than 5°, NPQ was corrected for using the average of two methods; chlorophyll being extrapolated to the surface using the backscattering channel as a guide (Sackmann et al., 2008) and assuming a constant raw chlorophyll concentration above the highest value found near the base of the mixed layer (Xing et al., 2012). The mixed layer depth definition used in these corrections uses a fixed density threshold criterion of 0.005 kg $m^{-3}$ from the surface (Johnson et al., 2017). SOCCOM also uses a sensor gain correction specific to the SO. While a gain correction of 2 has been accepted as a global factor for the WET Labs ECO FLBB sensor, Roesler et al. (2017) determined 6.4 to be more appropriate for the Southern Ocean.

For every profile, chlorophyll was averaged in the upper 10 meters of the water column. The surfacing locations were then matched with the nearest satellite or modelled parameter spatially and temporally to enable comparison. Mixed layer depths for each float profile were computed using the potential density difference from the surface (0-20m) of 0.03 kg $m^{-3}$ used in the Dong et al. (2008) study to enable comparison of MLD's from different sources. *In situ* density profiles were visually inspected with the corresponding computed MLDs to confirm this method's accuracy.

## 2.5 Bulk Richardson Number

A combination of the OSCAR surface current product and density profiles from SOCCOM floats were used to estimate a bulk Richardson number (Ri). The Richardson number was used as a criterion for determining if surface shear could cause mixing with a given ambient stratification:

$$4)\quad Ri = \frac{N^2}{S_h^2},$$

where N is the buoyancy frequency,

$$5)\quad N^2 = \frac{g}{\rho}\frac{\partial \rho}{\partial z},$$

and $S_h$ is the shear term,

$$6)\quad S_h^2 = \left(\frac{\partial u}{\partial z}\right)^2 + \left(\frac{\partial v}{\partial z}\right)^2 .$$

g is the acceleration due to gravity, ρ the potential density at the surface, $\frac{\partial \rho}{\partial z}$ the change in density from the surface down to a depth, and $\frac{\partial u}{\partial z}$ and $\frac{\partial v}{\partial z}$ are the change in horizontal and vertical velocity, respectively, over the same depth. When $Ri < 0.25$, turbulence will generate vertical mixing due to strong shear or weak stratification.

The Richardson number was calculated for every *in situ* profile after the SOCCOM floats' surfacing locations were matched with the coinciding OSCAR surface current estimates. This parameter was calculated with $\partial z$ as 30 meters because the OSCAR surface currents are representations of averaged flow over the upper 30 m of the ocean.

## 2.6 Probabilistic Model Development

Fifteen years (2003-2017) of matched KE and CHL data were parsed by month (December, January, February), sorted by KE, and divided evenly into 10 "bins", each containing 10% of the matched data. Kolmogorov-Smirnov tests (ks.test in R) were

used to determine if the distributions observed in each of the 10 KE bins statistically differed from one another (R Core Team 2017).

To further model the relationship between KE and CHL, an Expectation Maximization (EM) algorithm, from the mixtools package in R, was used to fit a mixture of univariate normal distributions to the observed data in each of the 10 KE bins (Benagalia et al., 2017). An EM algorithm is an iterative method to isolate maximum likelihood estimates of parameters for a mixture of two normal distributions describing an observed distribution. The EM algorithm is a two-step process, consisting of an expectation (E) step and a maximization (M) step. This algorithm uses the current parameter estimates to create a function for the expected log-likelihood, computes new parameters to maximize the expected log-likelihood, and continues to iterate until the log-likelihood is effectively maximized (Benagalia et al., 2017). The means, standard deviations, and mixing percentages for a mixture of two normal distributions observed in a true distribution were obtained by running this algorithm on each of the 10 KE bins. These EM estimates were then used as seed values in a non-linear least-squares model (nls in R) to estimate the nonlinear relationship between these mean, standard deviation, and mixing percentage curves for the two distributions as a function of KE (R Core Team 2017). Using the function rnormmix in R, these continuous functions were used to probabilistically predict surface chlorophyll concentrations for each KE measurement (Benagalia et al., 2017). This procedure was performed separately for December, January, and February.

### 2.7 Probabilistic Model Testing

The parameters for these monthly models were trained on a random 80% of the matched KE-CHL data from each month over the study period and tested on the

remaining 20% of the data from each month. Using the package lmodel2, a model II ranged major axis linear regression was performed to first assess the accuracy of the predicted binned mean chlorophyll and standard deviation against the observed binned mean chlorophyll and standard deviation, and for examining the relationship between climatologies of observed and predicted chlorophyll concentrations (Legendre, 2018).

### 2.8 KE-CHL Probabilistic Model Application

The results of the monthly probabilistic models were evaluated in several ways. Predictions were made for every 5-day averaged block of matched KE-CHL data using the appropriate monthly model. The probabilistic models were evaluated temporally by first comparing yearly climatologies of observed and predicted chlorophyll concentration. The means and total integrated chlorophyll from these yearly climatologies were compared. Because the observed MODIS chlorophyll product is a different resolution (9 km) than the OSCAR product (1/3°) used to make the chlorophyll predictions, it was necessary to use two different pixel-area weighted integrations. The probabilistic models were also evaluated spatially by comparing maps of averaged observed and predicted chlorophyll concentration over the 2003-2017 study period.

### 2.9 Evaluating KE and the Bulk Richardson Number in Relation to the MLD and CHL

The impact of kinetic energy on the mixed layer depth and chlorophyll concentration was evaluated in both the remotely sensed and *in situ* data sets. The same 10% binning procedure performed in the development of the monthly probabilistic models was performed on a dataset of matched KE, CHL, and MLD from the Argo float climatology. This same procedure was performed on an *in situ*

SOCCOM float dataset of MLD and CHL matched to OSCAR KE but with 20% bins because of the smaller sample size. One-way ANOVA's and "post-hoc" Tukey's multiple-comparison tests were used to test the impact that different levels of kinetic energy had on (remotely sensed and *in situ*) mixed layer depth and chlorophyll concentration (R Core Team 2017). After calculating bulk Richardson numbers for each SOCCOM float profile matched to a coinciding OSCAR surface current estimate, t-tests were used to statistically compare the mean mixed layer depth and chlorophyll concentration in the mixing or non-mixing profiles.

# Chapter 3

# RESULTS

## 3.1 Mesoscale Kinetic Energy and Phytoplankton Abundance

It appears that, throughout the entire SO as well, high levels of KE correspond with low phytoplankton abundance, while high phytoplankton abundance occurs only when KE is low (Figures 3.1 and 3.2). This pattern was consistent when observations were broken down by month (Dec, Jan, Feb) and was also observed in the *in situ* SOCCOM float observations (Figure 3.3) indicating that the general relationship is not an artefact of satellite observations. A model II regression showed there was a significant positive relationship (slope = 0.76, intercept = -0.13, $r^2 = 0.66$, $p << 0.001$) between matched satellite derived estimates of chlorophyll and mean *in situ* chlorophyll measurements in the upper 10 meters from SOCCOM floats in $\log_{10}$ space (Figure 3.4). This indicates that the SO specific chlorophyll algorithm does a satisfactory job of representing surface chlorophyll concentrations (Johnson et al., 2017).

One explanation for the lack of high CHL values at high KE is sampling bias. If both high KE and high CHL are rare, these two conditions may not be represented in the data. To confirm that this KE-CHL relationship is not due to a sampling bias, the 15 years of matched KE and CHL data was sorted by KE and then divided into 10 KE bins each containing 10% of the total data. If the pattern is due to sampling bias, these distributions would be self-similar. However, when the data is parsed by month, these distributions are not self-similar. KS tests revealed that every distribution of CHL in the KE bins were significantly different from one another ($p << 0.001$). Furthermore, these distributions also provide evidence that there is a seasonal component to this

KE-CHL relationship (Figure 3.5). As the season progresses from December to February, higher CHL shoulders form in the distributions occurring in the lower KE bins, while the CHL distribution in higher KE bins shifts to lower values.

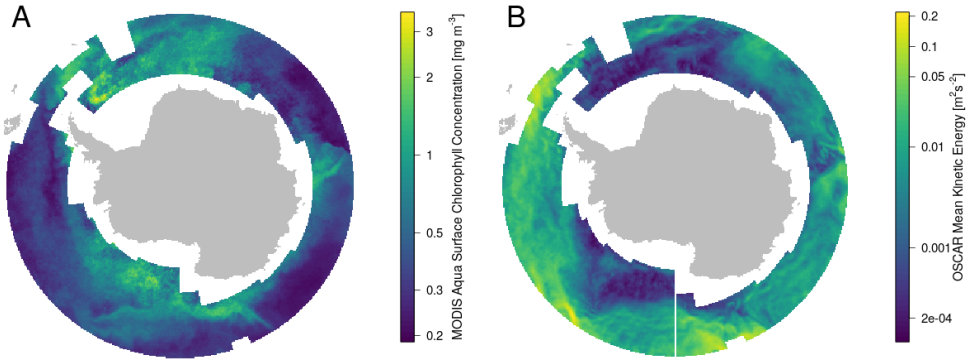


Figure 3.1: (A) Averaged MODIS *Aqua* surface chlorophyll concentration from 2003-2017. (B) Averaged mesoscale mean kinetic energy per unit mass derived from OSCAR surface currents.

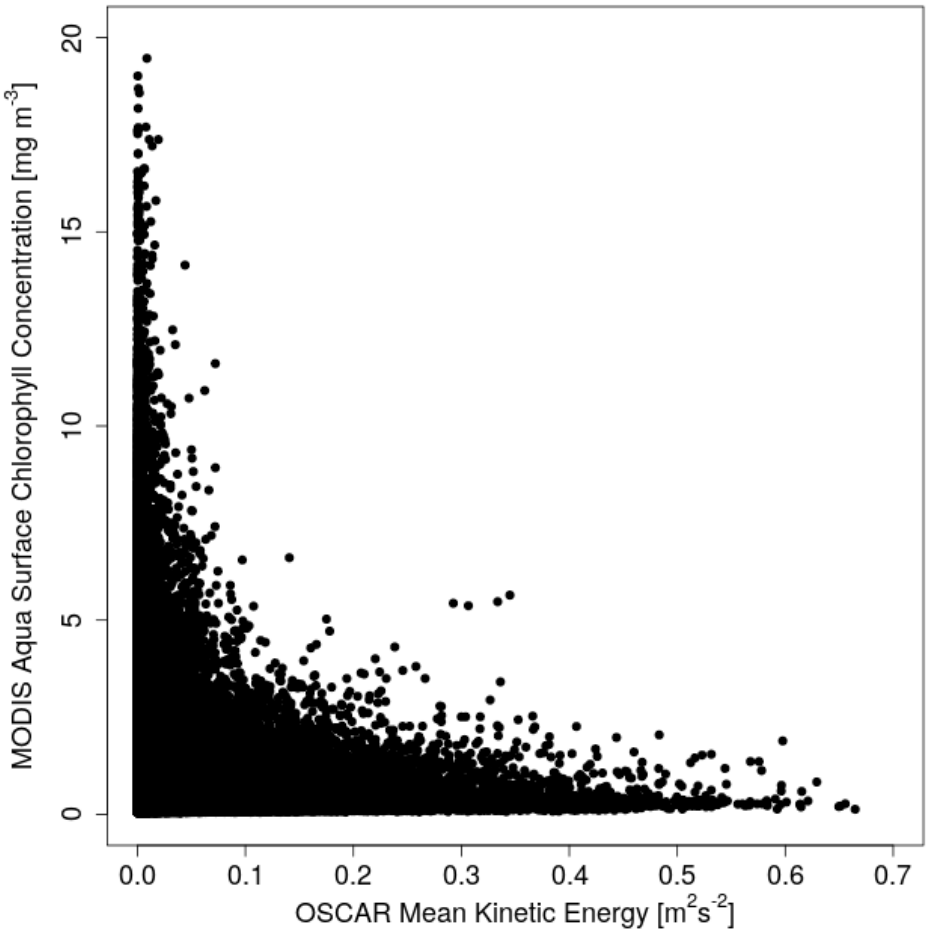


Figure 3.2: MODIS *Aqua* five-day composites of surface chlorophyll-a concentration with coincident estimates of surface mesoscale kinetic energy per unit mass from OSCAR surface currents.

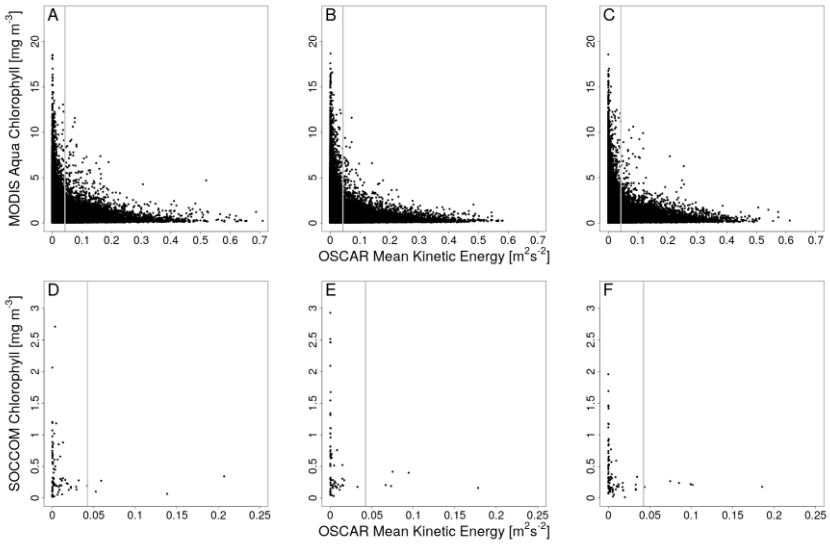


Figure 3.3: KE-CHL relationship broken down by month in the remotely sensed and *in situ* float data sets (December = Figures A and D, January = Figures B and E, February = Figures C and F). Grey bars are for visual reference to show transition from low to high KE regimes.

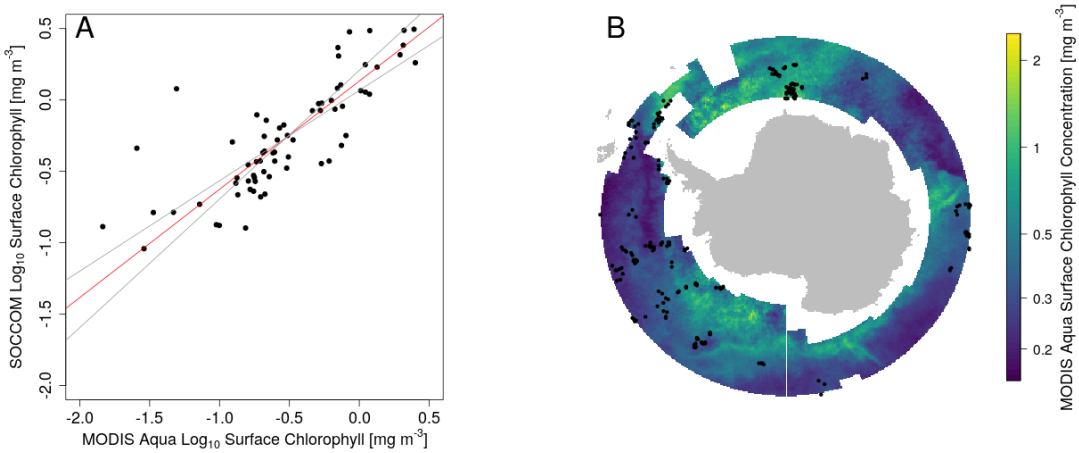


Figure 3.4: (A) Ranged major axis model II regression of MODIS *Aqua* surface chlorophyll concentration against SOCCOM surface chlorophyll concentration. (B) SOCCOM profile locations mapped against averaged MODIS *Aqua* surface chlorophyll concentration from 2003-2017.

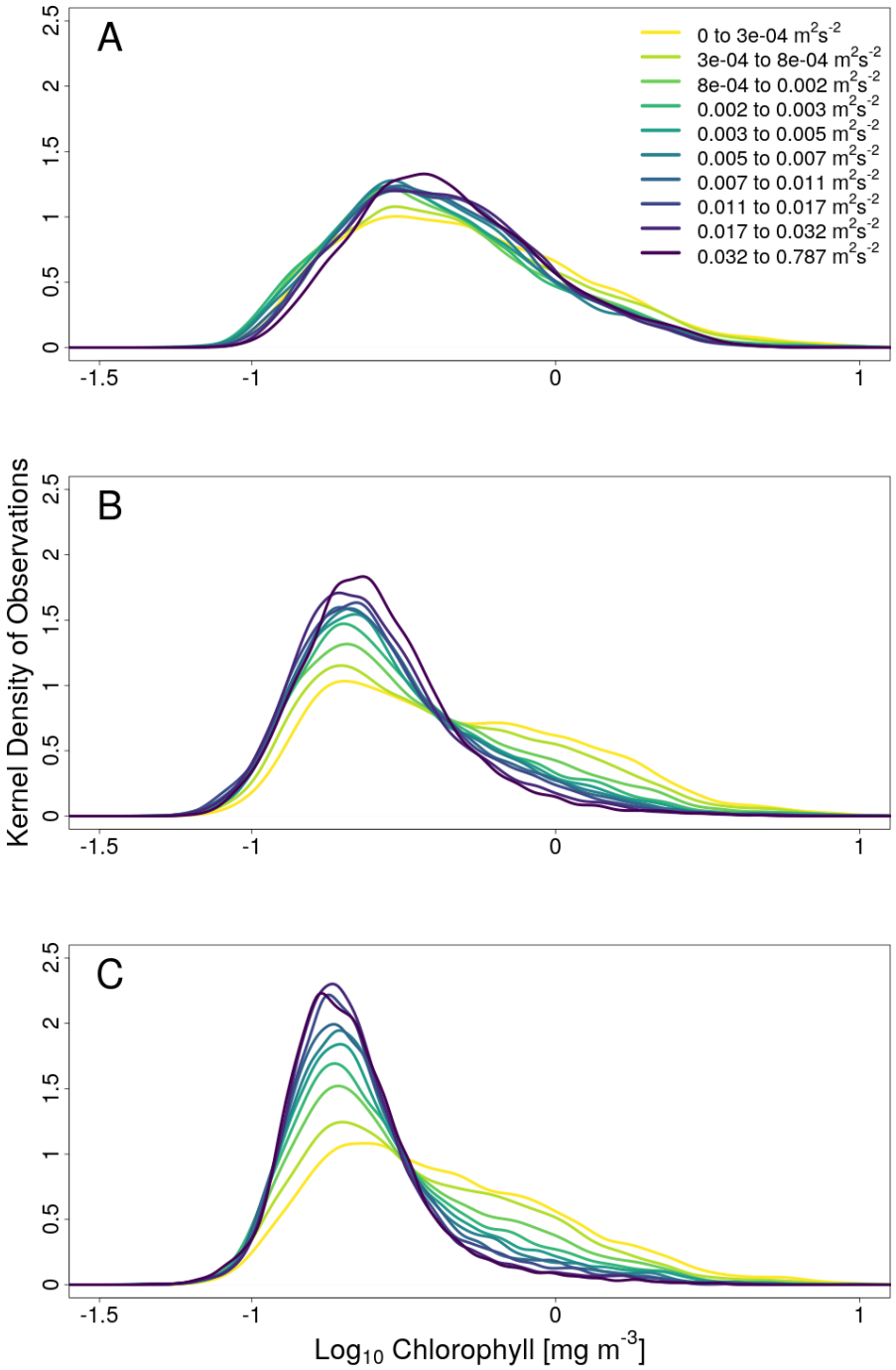


Figure 3.5: Density distributions of binned MODIS *Aqua* surface chlorophyll concentration with coincident OSCAR surface mean kinetic energy estimates. Each distribution contains 10% of the data for a given month (December = Figure A, January = Figure B, February = Figure C).

The results of the EM algorithm showed that these shouldered distributions could be modelled using a mixture of two normal distributions (Figure 3.6). I nominally term these distributions the "background" and "bloom" distributions, only to denote that one distribution has a higher mean than the other. The means, standard deviations and mixing percentages of these two distributions were either linear or hyperbolic functions of KE (Figure 3.7, Table 2). Table 3.1 shows parameters fit to these linear or hyperbolic functions of KE for the background and blooms distributions in each month:

7) Linear Fit: $Mean, SD, Mix\ \% = A * KE + B$

8) Hyperbolic Fit: $Mean, SD, Mix\ \% = \frac{A}{(B+KE)} + C$

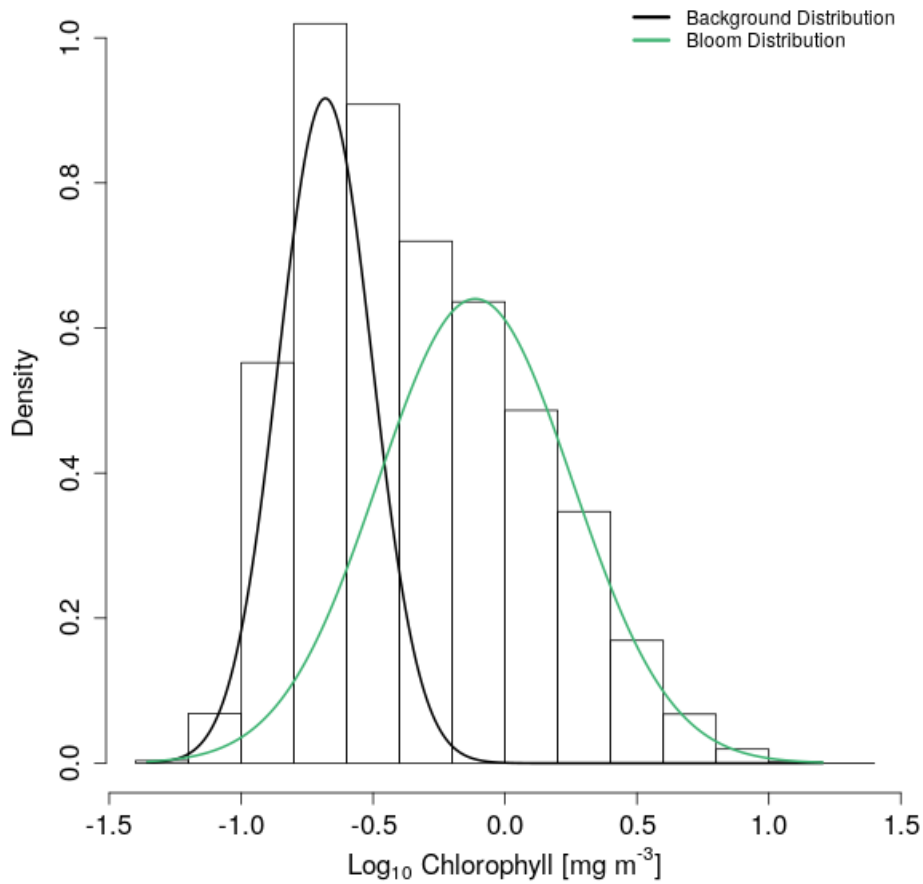


Figure 3.6: An example of the two distributions that have been fit to the observed distribution in one of the 10 kinetic energy bins using an EM algorithm in R. This distribution is from the lowest kinetic energy bin observed in February, hence the large bloom distribution component.

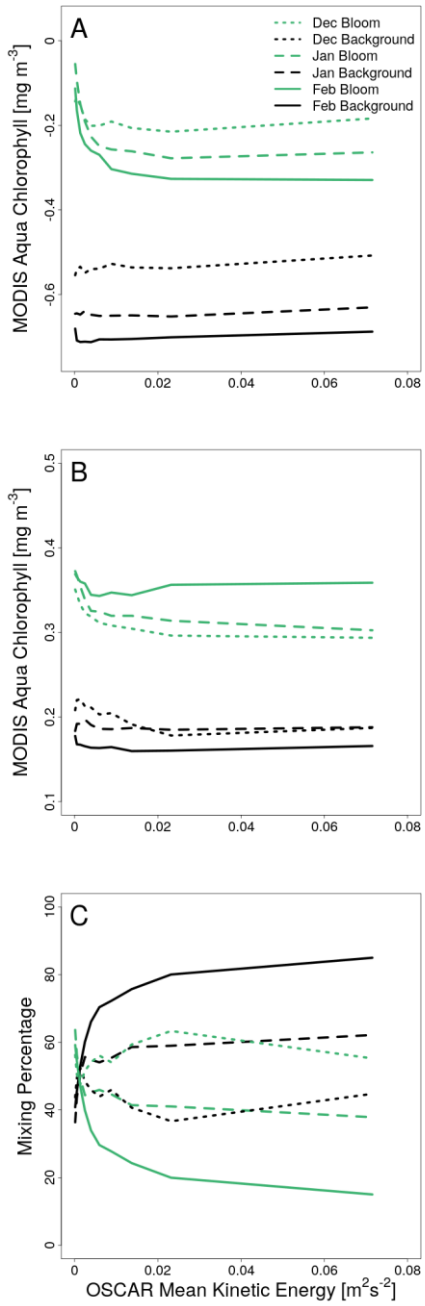


Figure 3.7: Mean (A), standard deviation (B), and mixing percentage (C) of the two distributions (bloom in green and background in black) describing the observed distribution in December (dotted line), January (dashed line), and February (solid line) as a function of kinetic energy.

Table 3.1: Parameters of linear or non-linear models fit to the means, standard deviations, and mixing percentages of the two distributions parsed by month. Hyperbolic functions of KE were fit in the non-linear models.

| Month | December | January | February |
|---|---|---|---|
| **Bloom Mean Fit** | *Hyperbolic* | *Hyperbolic* | *Hyperbolic* |
| **A Estimate** | 1.14E-04 | 3.44E-04 | 3.65E-04 |
| **A Standard Error** | 8.68E-05 | 5.46E-05 | 5.79E-05 |
| **B Estimate** | 1.36E-03 | 1.32E-03 | 1.54E-03 |
| **B Standard Error** | 1.13E-03 | 2.28E-04 | 2.61E-04 |
| **C Estimate** | -2.08E-01 | -2.86E-01 | -3.35E-01 |
| **C Standard Error** | 1.00E-02 | 6.46E-03 | 6.15E-03 |
| **Bloom Standard Deviation Fit** | *Hyperbolic* | *Hyperbolic* | *Linear* |
| **A Estimate** | 1.78E-04 | 1.71E-04 | 9.77E-03 |
| **A Standard Error** | 1.92E-05 | 3.89E-05 | 1.52E-01 |
| **B Estimate** | 2.86E-03 | 2.28E-03 | 3.54E-01 |
| **B Standard Error** | 3.04E-04 | 5.25E-04 | 3.71E-03 |
| **C Estimate** | 2.92E-01 | 3.04E-01 | NA |
| **C Standard Error** | 1.32E+03 | 3.14E-03 | NA |
| **Bloom Mixing Percentage Fit** | *Constant ** | *Hyperbolic* | *Hyperbolic* |
| **A Estimate** | NA | 2.01E-04 | 1.44E-03 |
| **A Standard Error** | NA | 6.25E-05 | 1.31E-04 |
| **B Estimate** | NA | 7.22E-04 | 3.07E-03 |
| **B Standard Error** | NA | 2.70E-04 | 2.72E-04 |
| **C Estimate** | NA | 4.03E-01 | 1.43E-01 |
| **C Standard Error** | NA | 1.09E-02 | 8.57E-03 |
| **Background Mean Fit** | *Linear* | *Linear* | *Linear* |
| **A Estimate** | 0.484277 | 1.95E-01 | 2.38E-01 |
| **A Standard Error** | 0.111408 | 8.22E-02 | 1.53E-01 |
| **B Estimate** | -0.54296 | -6.48E-01 | -7.06E-01 |
| **B Standard Error** | 0.002724 | 2.01E-03 | 3.74E-03 |
| **C Estimate** | NA | NA | NA |
| **C Standard Error** | NA | NA | NA |
| **Background Standard Deviation Fit** | *Hyperbolic* | *Linear* | *Hyperbolic* |
| **A Estimate** | 5.11E-04 | -4.04E-02 | 4.56E-06 |
| **A Standard Error** | 4.79E-04 | 6.62E-02 | 2.88E-06 |
| **B Estimate** | 1.14E-02 | 1.89E-01 | 1.65E-04 |
| **B Standard Error** | 8.90E-03 | 1.62E-03 | 1.94E-04 |
| **C Estimate** | 1.74E-01 | NA | 1.63E-01 |
| **C Standard Error** | 1.12E-02 | NA | 1.03E-03 |
| **Background Mixing Percentage Fit** | *Constant ** | *Hyperbolic* | *Hyperbolic* |
| **A Estimate** | NA | -2.01E-04 | -1.44E-03 |
| **A Standard Error** | NA | 6.25E-05 | 1.31E-04 |
| **B Estimate** | NA | 7.22E-04 | 3.07E-03 |
| **B Standard Error** | NA | 2.70E-04 | 2.72E-04 |
| **C Estimate** | NA | 5.97E-01 | 1.43E-01 |
| **C Standard Error** | NA | 1.09E-02 | 8.57E-03 |

The mixing percentages of the background and bloom distributions in January and February followed a hyperbolic model. However, this was not the case in December, in which there was no clear function that seemed best to approximate the mixing percentages of the background and bloom distribution. Since the mixing percentage of these two distributions was relatively constant across KE levels, the mixing percentage for these two distributions across different levels of KE is held constant. There was also no clear CHL shoulder at low KE present in December (Figure 3.5A), suggesting that the mixing percentage of these background and bloom distributions would have little effect on the model. These estimates of the mean, standard deviation, and mixing percentage for the background and bloom distributions were then used to probabilistically predict CHL from KE for December, January and February.

To test the performance of these monthly probabilistic models, models were fit on a random 80% of the data from each month, and tested on the remaining 20%. Because these are probabilistic models, I compared the observed and predicted mean, standard deviation, and distributions for each of the 10 KE bins for each month. Model II regression results comparing observed and modeled KE bin CHL means are not significantly different than a 1:1 line for January and February (January MA regression slope = 1.03, 95% CI = 0.98 – 1.07 & February MA regression slope = 0. 96, 95% CI = 0.88 – 1.06, Figure 3.8). The regression results for December is significantly different from a 1:1 line (MA regression slope = 0.52, Figure 3.8), but, the dynamic range of CHL data in December is very small, and therefore the slope is difficult to estimate. However, the overall predicted mean is within less than 1% of the observed mean in December. Furthermore, model II regression including all months

was not significantly different than a 1:1 line (MA regression slope = 0.99, 95% CI = 0.96-1.03) (Figure 3.8).

Model II regression results comparing the observed and modeled KE bin CHL standard deviations are not different than a 1:1 line for December, January, and February (December MA regression slope = 1.19, 95% CI = 0.99-1.35, January MA regression slope = 1.03, 95% CI = 0.96-1.09, February MA regression slope = 0.94, 95% CI = 0.88-1). Model II regression including all months was not significantly different than a 1:1 line either (MA regression slope = 0.98, 95% CI = 0.94-1.02) (Figure 3.8).

After comparing the observed and predicted mean and standard deviation for each of the 10 KE bins in each month, the distributions produced from probabilistic models were evaluated against the observed distributions (Figure 3.9). The predicted December distribution exhibited higher mean CHL in each bin and was more normally distributed than the January and February distributions as seen in the observed December distribution (Figures 3.9A & B). The predicted January and February distributions exhibit the same higher CHL shoulders in the lower KE bins and lower CHL values in the higher KE bins as seen in the observed January and February distributions (Figures 3.9C-F).

Further insight into this KE-CHL relationship was revealed through a comparison of yearly climatological mean and integrated, observed and predicted CHL (Figure 3.10). While the monthly models producing these predictions do not estimate the same interannual variability, they do capture the mean over the entire time series. The yearly means from the observed and predicted chlorophyll climatologies over the times series differed, on average, by approximately only 5%

and were not significantly different overall (t-test, p-value = 0.1086). Furthermore, the observed and predicted chlorophyll climatology integrations over the time series differed, on average, by approximately only 4%. The overall means from the integrations of observed and predicted chlorophyll climatologies were also not significantly different (t-test p-value = 0.2133).

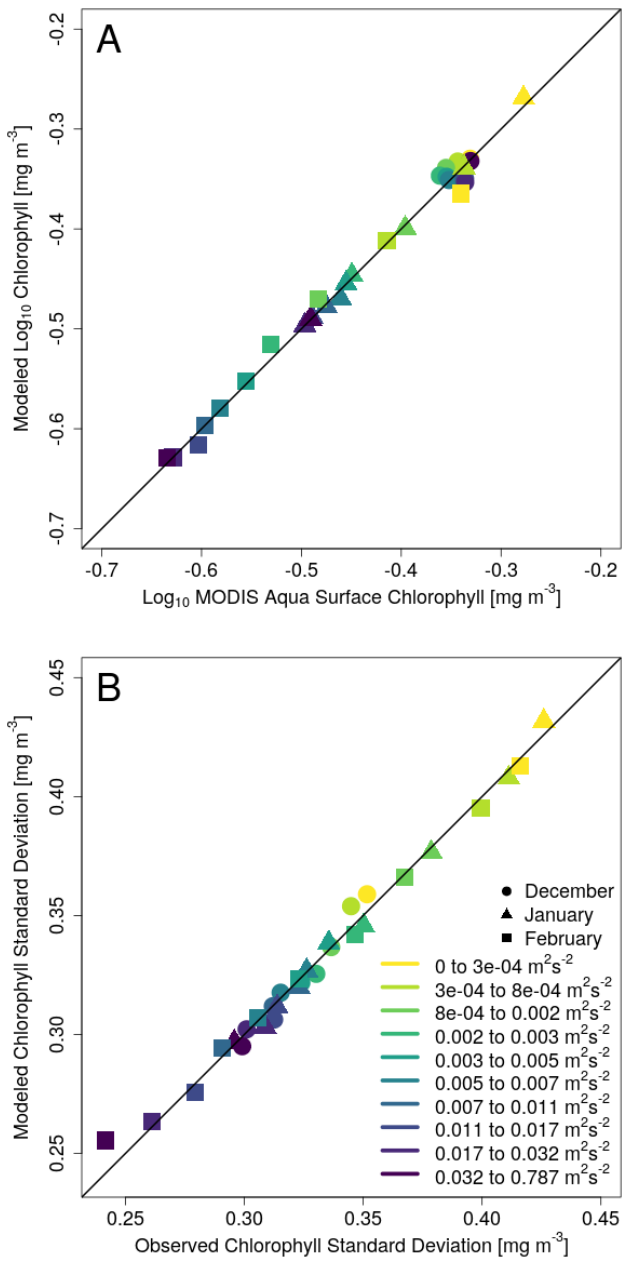


Figure 3.8: (A) Measured and predicted mean chlorophyll from each of the 10 kinetic energy bins for each monthly model. (B) Measured and predicted chlorophyll standard deviation from each of the 10 kinetic energy bins for each monthly model.

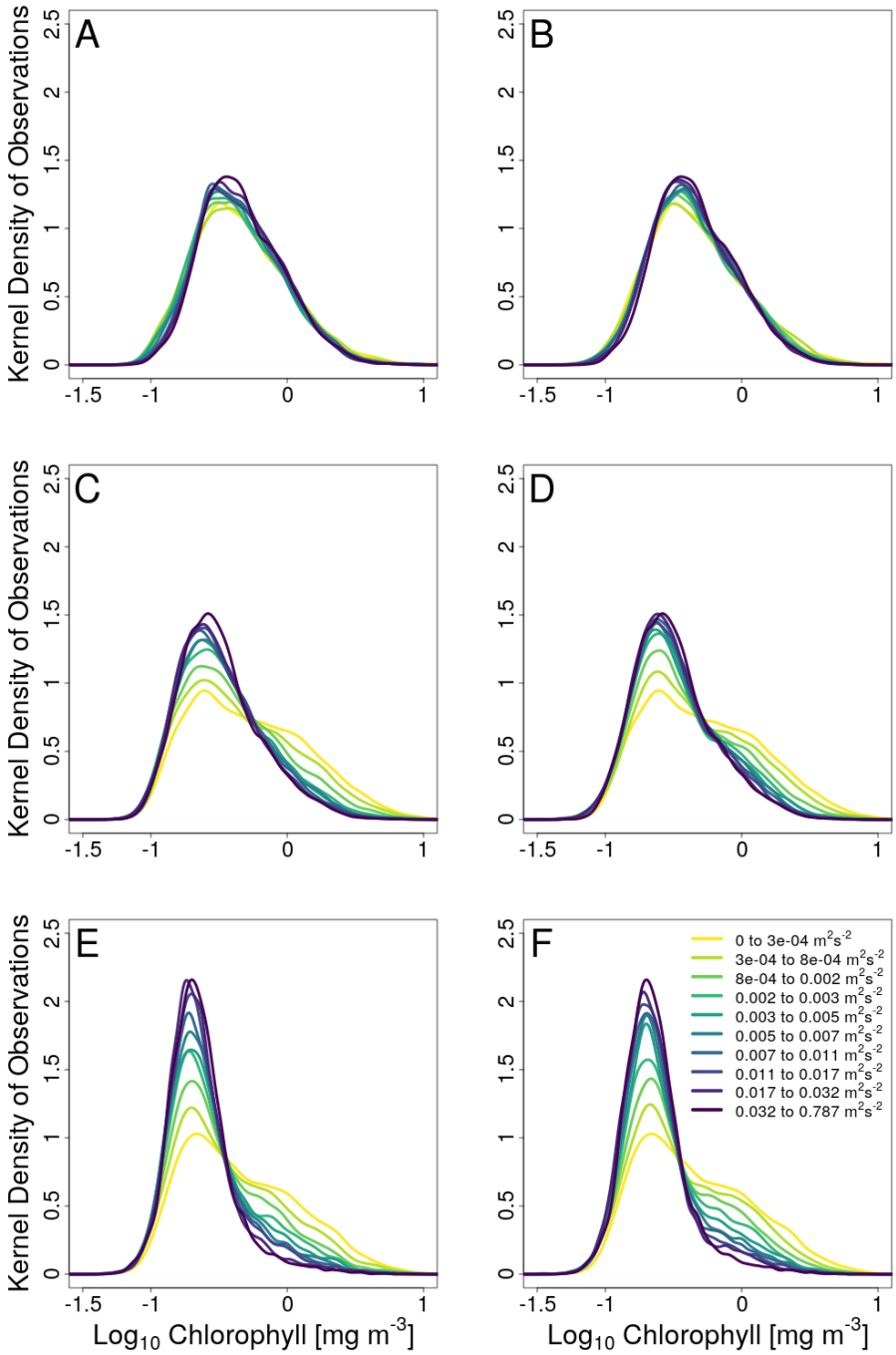


Figure 3.9: Left Column: Observed 10 distributions for the untrained 20% of the data by month (December = Figure A, January = Figure C, February = Figure E). Right Column: Modeled 10 distributions trained on 80% of the data by month and applied to the remaining 20% of data (December = Figure B, January = Figure D, February = Figure F).

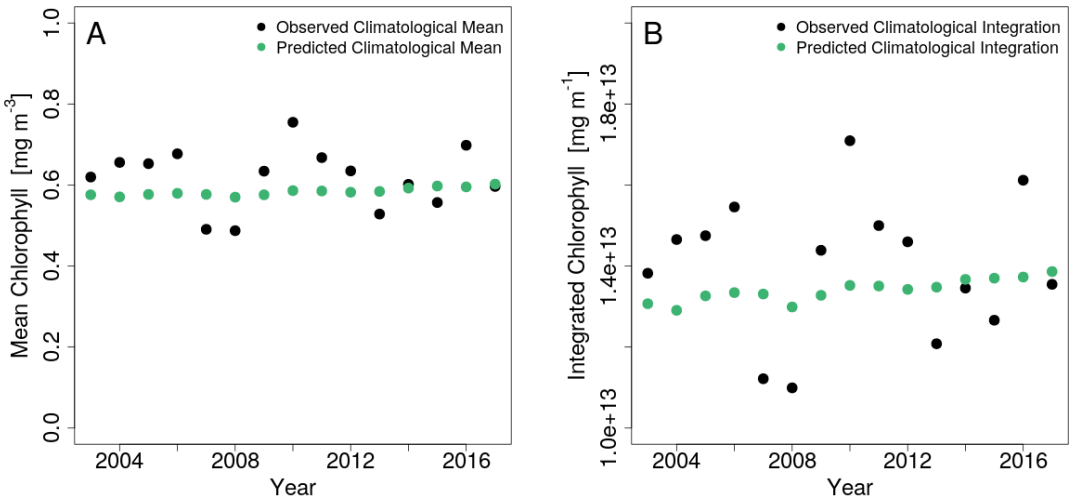


Figure 3.10: (A) Comparison of mean chlorophyll concentration from yearly climatologies of observed and predicted chlorophyll. (B) Comparison of total pixel-area weighted integrations of chlorophyll concentration from yearly climatologies of observed and predicted chlorophyll

## 3.2 Mesoscale Kinetic Energy as a Proxy for Mixed Layer Depth

Figure 3.11 shows the relationship between MODIS *Aqua* surface chlorophyll concentration, OSCAR kinetic energy, and mixed layer depths from the Dong et al. (2008) climatology throughout the entire Southern Ocean overall and separately in December, January, and February from 2003-2017. The 10 points in each panel of Figure 3.11 were generated according to the same 10% KE binning procedure as in Figure 3.5.

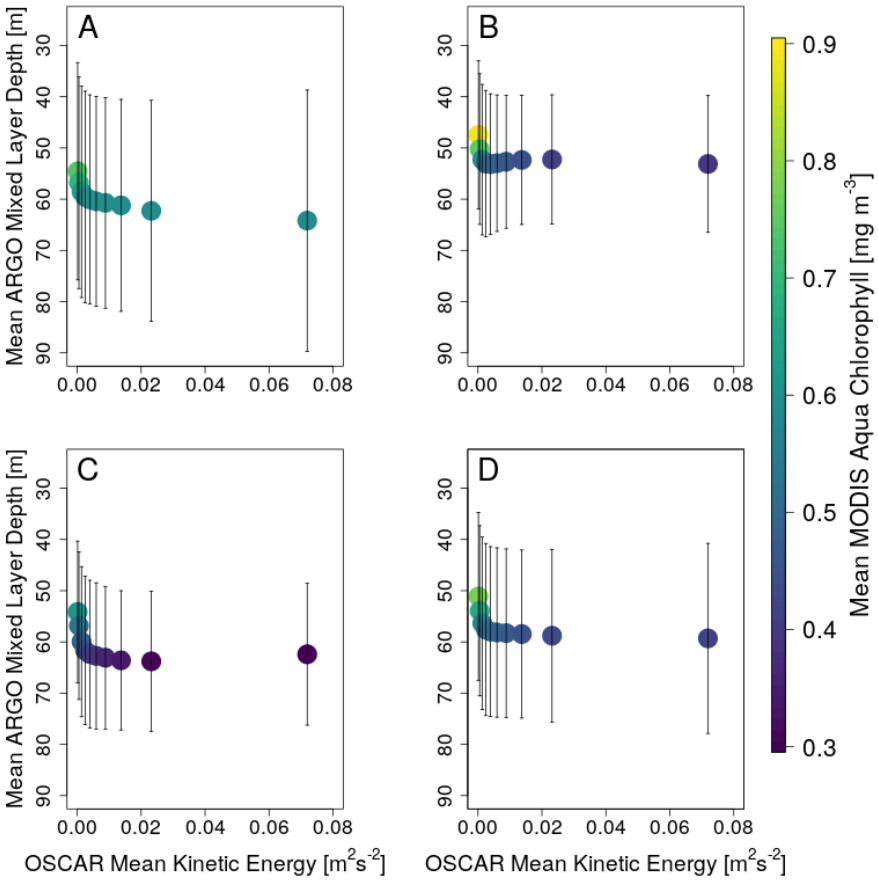


Figure 3.11: Compiled ARGO float mixed layer depths matched to OSCAR mean kinetic energy and colored by MODIS *Aqua* surface chlorophyll concentration in December (A), January (B), February (C), and overall (D). The 10 points in each panel are generated according to the same 10% binning procedure as in Figure 3.5 and error bars are one standard deviation.

Our analysis suggests that high kinetic energy is a proxy for deeper mixed layers and lower chlorophyll. In the overall data, the one-way ANOVA's indicated that mean kinetic energy had a statistically significant effect on the mixed layer depth and surface chlorophyll concentration (both p-values << 0.001). The results from the

Tukey's multiple-comparison test indicated that the mean chlorophyll concentration differed across every KE bin while the mean mixed layer depth different across every KE bin minus the pairs of bins 5 & 6, bins 6 & 7, and bins 7 & 8.

Specifically in December, the one-way ANOVA's indicated that mean kinetic energy had a statistically significant effect on the mixed layer depth and surface chlorophyll concentration (both p-values << 0.001). The results from the Tukey's multiple-comparison test indicated that the mean chlorophyll concentration differed across every KE bin minus the pair of bins 4 & 5, bins 5 & 6, bins 6 & 7, and bins 7 & 8. On the other hand, results from the Tukey's multiple-comparison test indicated that the mean mixed layer depth differed across every KE bin pair from bins 1-4 but not from every KE bin pair from bins 4-10 (All p-values << 0.001).

In January data, the one-way ANOVA's indicated that mean kinetic energy had a statistically significant effect on the mixed layer depth and surface chlorophyll concentration (both p-values << 0.001). The results from the Tukey's multiple-comparison test indicated that the mean chlorophyll concentration differed across every KE bin minus the pairs of bins 3 & 9, bins 4 & 5-6, bins 5 & 6, bins 7 & 8, and bins 9 & 10. On the other hand, the results from the Tukey's multiple-comparison test indicated that the mean mixed layer depth differed across every KE bin pair minus the pairs of bins 5 & 6 and bins 6 & 7 (All p-values << 0.001).

In February data, the one-way ANOVA's indicated that mean kinetic energy had a statistically significant effect on the mixed layer depth and surface chlorophyll concentration (both p-values << 0.001). The results from the Tukey's multiple-comparison test indicated that the mean chlorophyll concentration differed across every KE bin minus the pair of bins 5 & 10, bins 6 & 10, bins 5 & 6, bins 6 & 7, and

bins 8 & 9. On the other hand, the results from the Tukey's multiple-comparison test indicated that the mean chlorophyll concentration differed across every KE bin (All p-values << 0.001).

The *in situ* measurements from the SOCCOM floats revealed similar results which confirmed what was observed in the remotely sensed data. The same relationship observed in Figure 3.11 can be seen in Figure 3.12 but with SOCCOM surface chlorophyll concentration, OSCAR mean kinetic energy, and SOCCOM mixed layer depth throughout the entire Southern Ocean in December, January, February, and in these months combined. In all the months combined, the one-way ANOVA's indicated that mean kinetic energy had a statistically significant effect on the *in situ* mixed layer depth and surface chlorophyll concentration (both p-values << 0.001). The results from the Tukey's multiple-comparison test indicated that the mean *in situ* chlorophyll concentration and mixed layer depth from Bin 1 differed from that of each of the other bins but not across all other combinations (all p-values << 0.001).

Specifically in December, the one-way ANOVA's indicated that mean kinetic energy only has a statistically significant effect on *in situ* mixed layer depth (p-value = 0.0004). The results from the Tukey's multiple-comparison test indicated that the mean mixed layer depth differed from the pairs of KE bins 1 & 2 and bins 1 & 5 but not across all other combinations of bins (p-values = 0.007 & 0.004). KE not having a statistically significant effect on *in situ* CHL in December falls in line with the observed CHL distributions in each of the KE bins in the remotely sensed data in Figure 3.5.

In the January data, the one-way ANOVA's indicated that mean kinetic energy has a statistically significant effect on *in situ* mixed layer depth and surface

chlorophyll concentration (p-values = 0.0004 & 0.004). The results from the Tukey's multiple-comparison test indicated that the mean mixed layer depth differed across the pairs of KE bins 1 & 4 and bins 3 & 4 but not across all other combinations of bins (p-value = 0.0003 & 0.02). On the other hand, the results from the Tukey's multiple-comparison test indicated that the mean chlorophyll concentration differed only from the pair of KE bins 1 & 4 (p-value = 0.045).

In the February data, the one-way ANOVA's indicated that mean kinetic energy only has a statistically significant effect on *in situ* chlorophyll concentration (p-value << 0.001). The results from the Tukey's multiple-comparison test indicated that the mean chlorophyll concentration differed across every KE bin pair from bins 1-4 but not from every KE bin pair from bins 4-10 (p-values = 0.001, 0.0008, 0.02, & 0.00006 respectively).

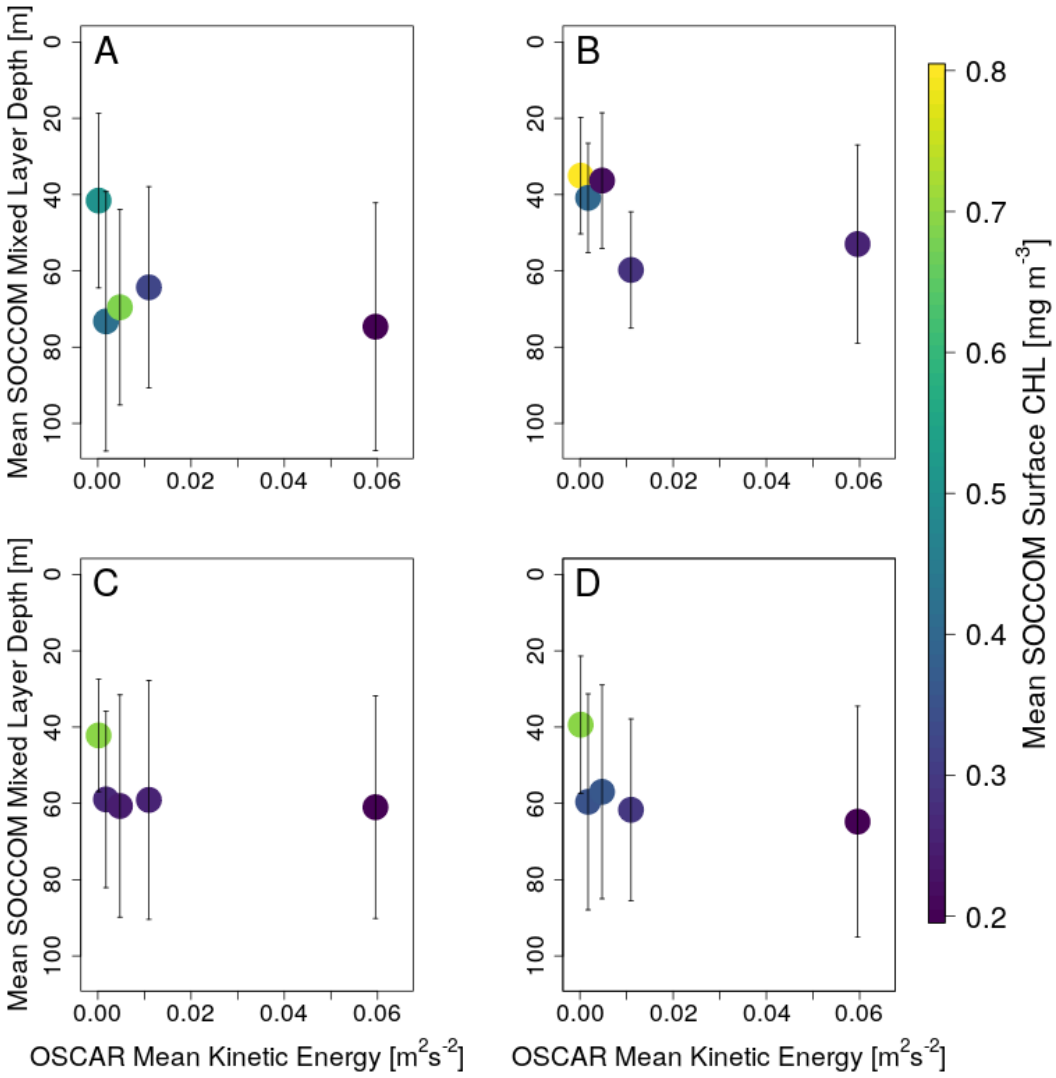


Figure 3.12: Compiled *in situ* mixed layer depth from SOCCOM floats matched to OSCAR mean kinetic energy and colored by *in situ* mean surface chlorophyll concentration in December (A), January (B), February (C), and overall (D). The 5 points in each panel are generated according to the same 10% binning procedure as in Figure 3.5 but into 20% bins to compensate for the difference in data points and error bars are one standard deviation..

Bulk Richardson numbers were calculated for every *in situ* profile after the SOCCOM floats' surfacing locations were matched with coinciding OSCAR surface current estimates. Out of these 266 profiles, 251 have coincident estimates of surface mean kinetic energy from the OSCAR product. When the bulk Richardson numbers were less than 0.25 (threshold for turbulent mixing), the mean chlorophyll concentration was observed to be 0.348 mg $m^{-3}$ while the mean chlorophyll concentration was observed to be 0.595 mg $m^{-3}$ when Richardson numbers were greater than 0.25 (t-test, p-value << 0.001, Figure 3.13). When bulk Richardson numbers were less than 0.25, the mean mixed layer depth was observed to be 82 m while the mean mixed layer depth was observed to be 56 m when Richardson numbers were greater than 0.25 (t-test, p-value << 0.001, Figure 3.13). The mean kinetic energy associated with Richardson numbers below 0.25 was observed to be 0.021 $m^2 s^{-2}$.

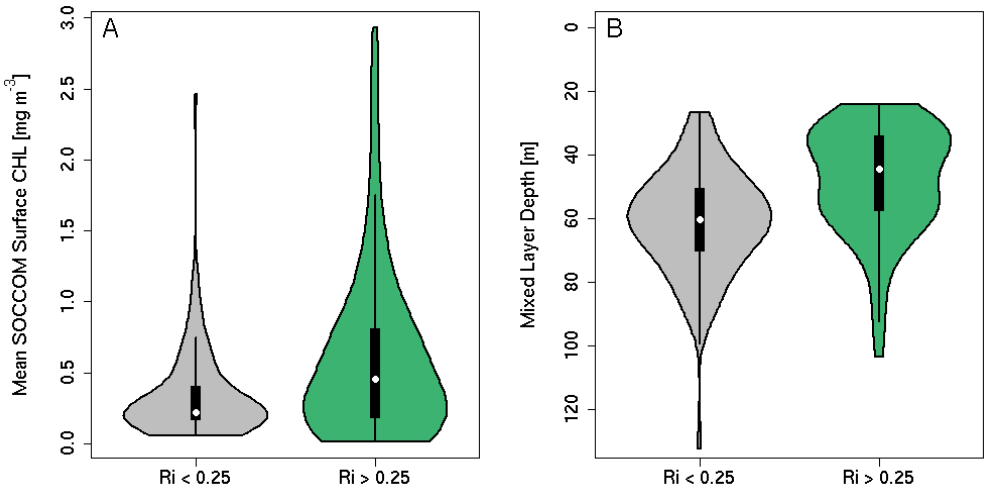


Figure 3.13: (A) Comparison of the distribution of SOCCOM surface CHL in float profiles with turbulent mixing (Ri < 0.25) and no turbulent mixing (Ri > 0.25). (B) Comparison of the distribution of mixed layer depth from SOCCOM float profiles with turbulent mixing (Ri < 0.25) and no turbulent mixing (Ri > 0.25). The black lines here indicate the 95% confidence interval, the black bars indicate the interquartile range, and the white dots indicate the median.

# Chapter 4

# DISCUSSION

In this study, I attempt to understand a unique relationship between mesoscale kinetic energy and surface chlorophyll concentration as it pertains to phytoplankton bloom dynamics within the Southern Ocean summer growing season. While there is much debate about the initiation of phytoplankton blooms in the SO and the importance of iron for phytoplankton here, I show that phytoplankton bloom dynamics within a growing season are dictated by the availability of light, mediated by changes in turbulent mixing and the mixed layer depth. I also show that KE can be used to probabilistically predict CHL in the SO and can be used as a proxy for the environmental conditions that permit bloom development.

Because the mean, standard deviation, and mixing percentage of the background and bloom distributions are a function of KE, KE can be used to probabilistically predict CHL. This is significant because of the differences in spatial and temporal coverage between the OSCAR surface current product and remotely sense chlorophyll concentration (Figure 2.2). The monthly probabilistic models produce predicted binned means and standard deviations that are not statistically different than the observed distributions (Figure 3.8). Furthermore, these models accurately reproduce the shapes of the observed distributions in each KE bin (Figure 3.9). While the predicted bin means for December differ slightly from the observed bin means, this is to be expected as they do not exhibit the same significant relationship with KE. Furthermore, when all the monthly data is combined, the overall predicted and observed binned chlorophyll means and standard deviations do not differ statistically from a 1:1 line. While the monthly models producing these

chlorophyll predictions do not capture the same variability in observed yearly climatological mean and integrated chlorophyll they do capture the mean over the entire time series (Figure 3.10).

In agreement with observations from Davies (2015) in the Drake Passage region, high phytoplankton abundance was not remotely sensed or observed *in situ* while kinetic energy was high throughout the entire Southern Ocean (Figures 3.2 and 3.3). Remotely sensed (Figure 3.11) and SOCCOM float observations (Figure 3.12) provide evidence suggesting that high levels of KE deepen the vertical structure of the water column which can limit phytoplankton abundance in several different manners. While turbulence driven (Huisman et al., 1999) and seasonally driven (Sverdrup, 1953) residence time in the euphotic zone can regulate phytoplankton abundance, these observations suggest a mesoscale light limitation as one of the potential explanations for why high KE limits phytoplankton abundance in the surface. Because both mixed layer depths and euphotic depths range from 20-100 meters during SO summers, it is plausible that high KE limits phytoplankton growth by reducing their time spent in the euphotic zone (Soppa et al., 2013). This explanation further implies that low KE may be a necessary, but not sufficient, precondition for phytoplankton blooms during the summer growing season.

Another possible explanation is simply higher KE leading to the dilution of CHL in the upper mixed layer, thus an apparent decrease in surface CHL. High KE's ability to deepen the mixed layer theoretically increases the volume over which phytoplankton can reside in the water column thus diluting their concentration in the water column. Figures 3.11 and 3.12 can be used to test if a dilution effect is a possible mechanism. This comparison can be done by taking the mean chlorophyll

concentration in the lowest KE bin, multiplying it by the mean mixed layer depth observed in that bin, and extrapolating that concentration over the mixed layer observed in the highest KE bin. In the December remotely sensed data (Figure 3.11A), the mean chlorophyll concentration (0.73 mg $m^{-3}$) in the weakest KE bin multiplied by the mean mixed layer depth from that bin (54 m) results in a concentration of approximately 40 mg $m^{-2}$. This concentration diluted over the 64 m mixed layer observed in the highest KE bin results in an approximate concentration of 0.62 mg $m^{-3}$, which is only slightly higher than the concentration of 0.59 mg $m^{-3}$ observed in this bin. In the December *in situ* data (Figure 3.12A), the mean chlorophyll concentration (0.5 mg $m^{-3}$) in the weakest KE bin multiplied by the mean mixed layer depth from that bin (41 m) results in a concentration of approximately 21 mg $m^{-2}$. This concentration diluted over the 74 m mixed layer observed in the highest KE bin results in an approximate concentration of 0.28 mg $m^{-3}$, which is slightly higher than the concentration of 0.19 mg $m^{-3}$ observed in this bin. Considering these examples as back-of-the-envelope calculations, a dilution effect is a plausible potential explanation behind this KE-CHL relationship in December. However, a dilution effect does not seem plausible in January or February as the computed, diluted chlorophyll concentration in the highest KE bins for these months are approximately two times greater than both the remotely sensed and *in situ* chlorophyll concentration observed in those bins. This suggests that higher KE in January and February leads deeper mixing and a more light-limited environment for phytoplankton rather than a simply just a dilution in their concentration in the water column.

It is clear the KE-CHL relationship is markedly different in December compared to both January and February. On average, the observed bin means in

December are higher than in January and February (Figures 3.5, 3.6, & 3.7). In addition to dilution, it is likely that this is due to the increasing seasonal availability of light, standing stock of nutrients, and the consequent seasonal timing of phytoplankton blooms throughout the Southern Ocean (Thomalla et al., 2011). That is, in December KE has less of an effect on phytoplankton abundance because as light becomes available phytoplankton will utilize the available nutrients, leaving a more nutrient (iron) limited environment in January and February (Tagliabue et al., 2014).

Sverdrup's critical depth hypothesis proposes spring blooms are caused by a shoaling of the mixed layer depth to some depth above a critical depth, resulting in improved light conditions for phytoplankton. As Franks (2014) notes, Sverdrup was actually referring to a "turbulent layer" when he wrote about a "mixed layer" and that this distinction has been forgotten in most tests of the critical depth hypothesis. While the *mixed layer depth* refers to the shallowest depth where some difference in temperature or density, usually measured from the surface, reaches a particular threshold, the *turbulent layer* is almost always equal to or shallower than the mixed layer as it contains waters that are kept in motion through active turbulence (Franks, 2014). The presence of a turbulent layer and its distinction from the mixed layer is relevant because it almost always leads to a violation in the first assumption of Sverdrup's critical depth hypothesis; that there is a *thoroughly* mixed top layer that vertically distributes phytoplankton evenly. Therefore, the turbulent layer is an important aspect to consider in terms of the potential mechanisms behind this KE-CHL relationship, especially if KE is a proxy for turbulent mixing. When there is vertical mixing within a turbulent layer, light water is pushed downward and heavy water is brought upwards. This process increases a water column's center of gravity

and potential energy, while dissipating kinetic energy. Therefore, there must be a source of kinetic energy strong enough to overcome the ambient density stratification to generate mixing along a density gradient. To investigate this, bulk Richardson numbers were calculated for 251 SOCCOM float profiles that had coincident estimates of surface mean kinetic energy from the OSCAR product. These Richardson numbers (Ri < 0.25) indicated that high kinetic energy could generate vertical mixing due to either strong shear or weak stratification. The bulk Richardson numbers were calculated with a $\partial z$ = 30 meters because the OSCAR surface currents are representations of averaged flow over the upper 30 m of the Ocean. The mean chlorophyll concentration in profiles were the Richardson number indicated vertical mixing (Ri < 0.25) was significantly lower, 0.348 mg $m^{-3}$, than in profiles where there was no vertical mixing, 0.595 mg $m^{-3}$, even when the Richardson number was only calculated to this depth. While there is clear evidence that high KE (i.e. Richardson numbers < 0.25) has the potential to deepen the mixed layer, there is also compelling evidence that high KE can generate a turbulent layer within a deep mixed layer thus still potentially effecting the localized residence time of phytoplankton in the euphotic zone. In other words, KE is a proxy for mixing, where higher KE leads to deeper mixing; that is, a gradient of turbulence through which phytoplankton are kept in motion and subjected to a gradient of light that exponentially decreases with depth. Even in a "thoroughly mixed" layer, defined by homogenized hydrographic properties, there is a vertical gradient in turbulence, highlighting the importance of KE's impact on phytoplankton due to its ability to generate vertical mixing.

This KE-CHL relationship implies that there may be regions of the Southern Ocean that are unlikely to support phytoplankton blooms because of consistently high

KE leads to deep turbulent mixed layers, even if other limiting factors such as iron are alleviated. Because low KE during January and February seems to be a precondition for phytoplankton abundance, regions of consistently high KE would also be unsuitable for large-scale iron fertilization experiments. In fact, it appears that the successful large-scale iron addition experiments (Boyd et al., 2000; Coale et al., 2004; Gervais at al., 2002; Hoffmann et al., 2006, Smetacek et al., 2012) were preferentially conducted in low KE environments (Table 4.1).

The probabilistic models of CHL from KE provide further evidence supporting the case that KE structures the spatial distribution of CHL in the Southern Ocean. Figure 4.1 shows a comparison of monthly MODIS *Aqua* CHL climatologies from 2003-2017 and a corresponding monthly climatology of CHL predictions from the monthly probabilistic models. Regression analysis of these data sets reveals that, in all the months combined, probabilistic predictions of CHL based on KE alone can explain 30% of the observed spatial variability in phytoplankton abundance (RMA regression slope = 0.323, intercept = -0.139, $R^2$ = 0.300). In January and February, these models explain 19% and 23% of the observed spatial variability in phytoplankton abundance (RMA regression slope = 0.397 & 0.459 &, intercept = -0.115 & -0.147, $R^2$ = 0.186 & 0.234). The regression between the climatologies of observed and predicted CHL in December are not significant ($R^2$ = 0.002), this is to be expected as the dynamic range of CHL in December is very small and KE does not have a statistically significant effect on CHL, likely because the system is undergoing the alleviation of seasonal light limitation.

Table 4.1: Estimated mesoscale kinetic energy during iron fertilization experiments in the Sothern Ocean. The surface mesoscale kinetic energy per unit mass (KE) is estimated at the latitude and longitude locations corresponding to each iron fertilization experiment. Shown are the KE ranges estimates over the duration of each experiment. The iron fertilization experiments conducted in the Southern Ocean are SOIREE (Boyd et al., 2000), EisenEx (Gervais et al., 2002), SoFex South and North (Coale et al., 2004), and EIFEX (Hoffmann et al., 2006). The KE is not available at the SOIREE study location. The experiment site selection for each study is summarized in the notes, along with any supplemental information about the environmental conditions or experiment. Table from Davies et al. (2015).

| Study | Latitude | Longitude | KE ($m^2s^{-2}$) | Notes |
|---|---|---|---|---|
| SOIREE | 61.0° S | 220.0° E | N/A | This site was chosen in-part due to "low eddy activity" and "low horizontal shear." |
| EisenEx | 48.0° S | 21.0° E | 0.00141-0.01082 | The iron injection was inside a mesoscale eddy to ensure "stable hydrographic conditions." |
| SoFEX South | 66.5° S | 188.2° E | 0.00173-0.00337 | A coherent patch was present throughout the experiment and slowly grew from 225 $km^2$ to 2,100 $km^2$ |
| SoFEX North | 56.2° S | 188.0° E | 0.00578-0.0462 | Strong horizontal shear stretched the patch into an "elongated filament" 7 km wide by 340 km long. |
| EIFEX | 50.0° S | 2.0° E | 0.00089-0.0578 | The iron injection was inside an eddy to ensure a "relatively stable water mass." Iron injections were on experiment days 0 and 15. The initial iron injection nearly doubled the observed chlorophyll-*a* concentration inside the eddy. However, the day 15 injection was followed by a plateau or slight dip in the observed chlorophyll-*a* concentration which is at a time when we estimate the KE peaked (~ experiment day 20). |

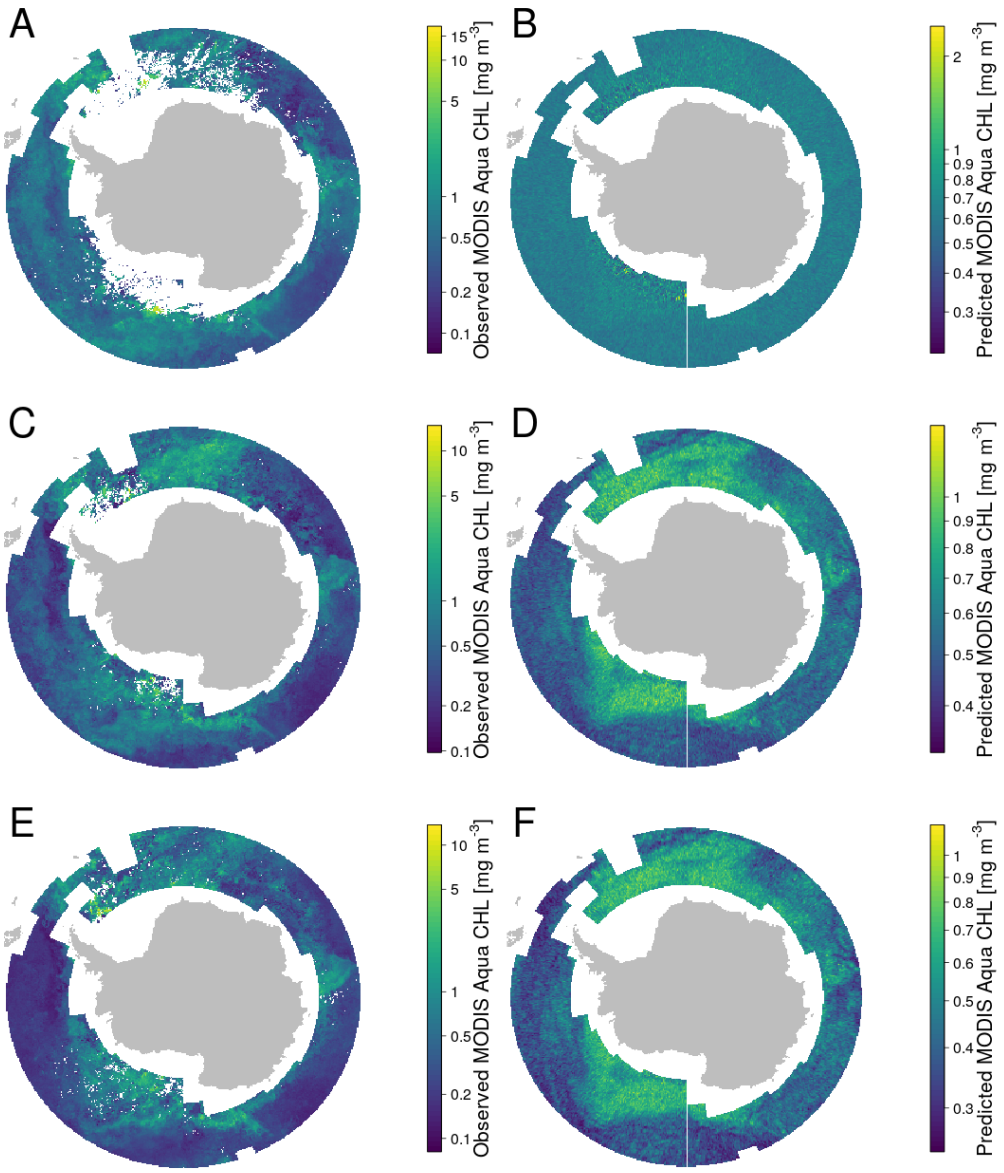


Figure 4.1: Climatology made from 5-day composites of MODIS *Aqua* surface chlorophyll concentration from 2003-2017 for December (A), January (C), and February (E). Climatology made from chlorophyll predictions from appropriate monthly models using 5-day composites of OSCAR mean kinetic energy from 2003-2017 for December (B), January (D), and February (F).

This study attempts to understand the unique influence surface mesoscale kinetic energy has on phytoplankton abundance in the Southern Ocean during the austral summer growing season. High levels of kinetic energy correspond with low phytoplankton abundance while high phytoplankton abundance occurs only when kinetic energy is low. I found that high levels of kinetic energy can generate vertical turbulence which has the potential to deepen the mixed layer. This vertical turbulence has been shown to limit phytoplankton growth, potentially through a dilution effect in December and a mesoscale light limitation in January and February. I also found that kinetic energy can be used in a probabilistic model to estimate chlorophyll concentration to a high degree of accuracy. These findings suggest that low surface mesoscale kinetic energy is a precondition for phytoplankton growth and can be used as a proxy for the environmental conditions that permit bloom development.

While the Southern Ocean's importance in the carbon cycle is an area of active research and discussion, several studies estimate that the SO could account for anywhere from a tenth to a quarter of the annual global ocean carbon uptake (McNeil & Matear, 2007; Roy et al., 2003; Takahashi et al., 2002). Over the next century, SO surface waters are expected to experience increased warming, shallowing of mixed layer depths, increases in light, and changes in upwelling and nutrient fluxes (Deppeler & Davidson, 2017; IPCC, 2013). As a result, phytoplankton productivity is expected to increase and the biological pump in the SO is expected to have a larger role in carbon sequestration (Sarmiento et al., 1998), assuming light is the major driver of productivity. However, these projections do not consider sub-seasonal, suppression of CHL due to the mesoscale effects discussed here. For one, it is important for future projections to include the relationship between mesoscale kinetic energy and

phytoplankton abundance because KE has now been shown to have the unique ability to structure the spatial variability in CHL. Furthermore, because of the spatial and temporal coverage in these KE estimates and KE's ability to accurately, probabilistically predict CHL, this relationship has the potential to provide insights into the full inventory of CHL in the SO. Therefore, it is only by incorporating this KE-CHL relationship, to fully understand the mechanisms that dictate phytoplankton growth, that forecasts will be able to accurately project future changes in our climate.

## REFERENCES


Arrigo, K. R., Dijken, G. L., & Bushinsky, S. (2008). Primary production in the Southern Ocean, 1997–2006. *Journal of Geophysical Research,113*(C8). doi:10.1029/2007jc004551

Atlas, R., Hoffman, R. N., Bloom, S. C., Jusem, J. C., & Ardizzone, J. (1996). A Multiyear Global Surface Wind Velocity Dataset Using SSM/I Wind Observations. *Bulletin of the American Meteorological Society,77*(5), 869-882. doi:10.1175/1520-0477(1996)0772.0.co;2

Behrenfeld, M. J. (2010). Abandoning Sverdrup's Critical Depth Hypothesis on phytoplankton blooms. *Ecology,91*(4), 977-989. doi:10.1890/09-1207.1

Benaglia, T., Chauveau, D., Hunter, D. R., & Young, D. (2009). Mixtools: An R Package for Analyzing Finite Mixture Models. *Journal of Statistical Software,32*(6). doi:10.18637/jss.v032.i06

Bonjean, F., & Lagerloef, G. S. (2002). Diagnostic Model and Analysis of the Surface Currents in the Tropical Pacific Ocean. *Journal of Physical Oceanography,32*(10), 2938-2954. doi:10.1175/1520-0485(2002)0322.0.co;2

Bopp, L., Aumont, O., Cadule, P., Alvain, S., & Gehlen, M. (2005). Response of diatoms distribution to global warming and potential implications: A global model study. *Geophysical Research Letters,32*(19). doi:10.1029/2005gl023653

Boyd, P. W., Jickells, T., Law, C. S., Blain, S., Boyle, E. A., Buesseler, K. O., et al. (2007). Mesoscale Iron Enrichment Experiments 1993-2005: Synthesis and Future Directions. *Science,315*(5812), 612-617. doi:10.1126/science.1131669

Boyd, P. W., Watson, A. J., Law, C. S., Abraham, E. R., Trull, T., Murdoch, R., et al. (2000). A mesoscale phytoplankton bloom in the polar Southern Ocean stimulated by iron fertilization. *Nature,407*(6805), 695-702. doi:10.1038/35037500

Ciais, P., Sabine, C., Bala, G., Bopp, L., Brovkin, V., Canadell, J., et al. (2013). Carbon and Other Biogeochemical Cycles. In: Climate Change 2013: The Physical Science Basis. Contribution of Working Group I to the Fifth Assessment Report of the Intergovernmental Panel on Climate Change [Stocker, T.F., D. Qin, G.-K. Plattner, M. Tignor, S.K. Allen, J. Boschung, A. Nauels, Y. Xia, V. Bex and P.M. Midgley (eds.)]. Cambridge University Press, Cambridge, United Kingdom and New York, NY, USA

Coale, K. H., Johnson, K.S., Chavez, F.P., Buesseler, K.O., Barber, R.T., Brzezinski, M.A., et al. (2004). Southern Ocean Iron Enrichment Experiment: Carbon Cycling in High- and Low-Si Waters. *Science,304*(5669), 408-414. doi:10.1126/science.1089778

Cota, G. F., Harrison, G.W., Platt, T., Sathyendranath, S., Stuart, V. (2003). Bio-optical properties of the Labrador Sea. *Journal of Geophysical Research,108*(C7). doi:10.1029/2000jc000597

Daniault, N., & Ménard, Y. (1985). Eddy kinetic energy distribution in the Southern Ocean from altimetry and FGGE drifting buoys. *Journal of Geophysical Research,90*(C6), 11877. doi:10.1029/jc090ic06p11877

Davies, A. R. (2015). On the sub-seasonal processes controlling the natural phytoplankton abundance and biological pump in the Drake Passage (Unpublished master's thesis). University of Delaware.

de Baar, H. J. W., Boyd, P.W., Coale, K.H., Landry, M.R., Tsuda, A., Assmy, P., et al. (2005), Synthesis of iron fertilization experiments: From the Iron Age in the Age of Enlightenment, *J. Geophys. Res.*, 110, C09S16, doi: 10.1029/2004JC002601.

Deppeler, S. L., & Davidson, A. T. (2017, February 02). Southern Ocean Phytoplankton in a Changing Climate. Retrieved from https://doi.org/10.3389/fmars.2017.00040

Dierssen, H. M., & Smith, R. C. (2000). Bio-optical properties and remote sensing ocean color algorithms for Antarctic Peninsula waters. *Journal of Geophysical Research: Oceans,105*(C11), 26301-26312. doi:10.1029/1999jc000296

Dong, S., Sprintall, J., Gille, S. T., & Talley, L. (2008). Southern Ocean mixed-layer depth from Argo float profiles. *Journal of Geophysical Research,113*(C6). doi:10.1029/2006jc004051

El-Sayed, S. (1984). Productivity of the Antarctic waters—A reappraisal. *Marine Phytoplankton and Productivity Lecture Notes on Coastal and Estuarine Studies,*19-34. doi:10.1029/ln008p0019

Esaias, W., Abbott, M., Barton, I., Brown, O., Campbell, J., Carder, K., et al. (1998). An overview of MODIS capabilities for ocean science observations. *IEEE Transactions on Geoscience and Remote Sensing,36*(4), 1250-1265. doi:10.1109/36.701076

ESR. 2009. OSCAR third degree resolution ocean surface currents. Ver. 1. PO.DAAC, CA, USA. Dataset accessed 2017-08-02 at http://dx.doi.org/10.5067/OSCAR-03D01.

Falkowski, P., Scholes, R. J., Boyle, E., Canadell, J., Canfield, D., Elser, J., et al. (2000). The Global Carbon Cycle: A Test of Our Knowledge of Earth as a System. *Science*,*290*(5490), 291-296. doi:10.1126/science.290.5490.291

Falkowski, P. G., & Raven, J. A. (2007). *Aquatic photosynthesis*. Princeton, NJ: Princeton Univ. Press.

Farmer, D. M., McNeil, C. L., & Johnson, B. D. (1993). Evidence for the importance of bubbles in increasing air–sea gas flux. *Nature*,*361*(6413), 620-623. doi:10.1038/361620a0

Franks, P. J. (2014). Has Sverdrup's critical depth hypothesis been tested? Mixed layers vs. turbulent layers. *ICES Journal of Marine Science: Journal Du Conseil*,*72*(6), 1897-1907. doi:10.1093/icesjms/fsu175

Gervais, F., Riebesell, U., & Gorbunov, M. Y. (2002). Changes in primary productivity and chlorophyll a in response to iron fertilization in the Southern Polar Frontal Zone. *Limnology and Oceanography*,*47*(5), 1324-1335. doi:10.4319/lo.2002.47.5.1324

Gregg, W. W., & Casey, N. W. (2004). Global and regional evaluation of the SeaWiFS chlorophyll data set. *Remote Sensing of Environment*,*93*(4), 463-479. doi:10.1016/j.rse.2003.12.012

Hoffmann, L. J., Peeken, I., & Lochte, K. (2007). Effects of iron on the elemental stoichiometry during EIFEX and in the diatoms *Fragilariopsis kerguelensis*and *Chaetoceros dichaeta*. *Biogeosciences Discussions*,*4*(1), 249-275. doi:10.5194/bgd-4-249-2007

Huisman, J., Oostveen, P. V., & Weissing, F. J. (1999). Critical depth and critical turbulence: Two different mechanisms for the development of phytoplankton blooms. *Limnology and Oceanography*,*44*(7), 1781-1787. doi:10.4319/lo.1999.44.7.1781

IPCC, 2013: Climate Change 2013: *The Physical Science Basis. Contribution of Working Group I to the Fifth Assessment Report of the Intergovernmental Panel on Climate Change* [Stocker, T.F., D. Qin, G.-K. Plattner, M. Tignor, S.K. Allen, J. Boschung, A. Nauels, Y. Xia, V. Bex and P.M. Midgley (eds.)]. Cambridge University Press, United Kingdom and New York, NY, USA, 1535 pp, doi:10.1017/CBO9781107415324.

Johnson, K. S., Plant, J. N., Coletti, L. J., Jannasch, H. W., Sakamoto, C. M., Riser, et al. (2017). Biogeochemical sensor performance in the SOCCOM profiling float array. *Journal of Geophysical Research: Oceans,122*(8), 6416-6436. doi:10.1002/2017jc012838

Johnson, R., Strutton, P. G., Wright, S. W., Mcminn, A., & Meiners, K. M. (2013). Three improved satellite chlorophyll algorithms for the Southern Ocean. *Journal of Geophysical Research: Oceans,118*(7), 3694-3703. doi:10.1002/jgrc.20270

Kahru, M., & Mitchell, B. G. (1999). Empirical chlorophyll algorithm and preliminary SeaWiFS validation for the California Current. *International Journal of Remote Sensing,20*(17), 3423-3429. doi:10.1080/014311699211453

Large, W. G., & Pond, S. (1981). Open Ocean Momentum Flux Measurements in Moderate to Strong Winds. *Journal of Physical Oceanography,11*(3), 324-336. doi:10.1175/1520-0485(1981)0112.0.co;2

Legendre, P. (2018) lmodel2: Model II Regression. R package version 1.7-3

Martin, J. H. (1990). Glacial-interglacial CO2change: The Iron Hypothesis. *Paleoceanography,5*(1), 1-13. doi:10.1029/pa005i001p00001

McNeil, B. I., & Matear, R. J. (2007). Climate change feedbacks on future oceanic acidification. *Tellus B,59*(2). doi:10.3402/tellusb.v59i2.16980

Moore, J. K., & Abbott, M. R. (2000). Phytoplankton chlorophyll distributions and primary production in the Southern Ocean. *Journal of Geophysical Research: Oceans,105*(C12), 28709-28722. doi:10.1029/1999jc000043

Pagano, T. S., & Durham, R. M. (1993). Moderate Resolution Imaging Spectroradiometer (MODIS). *Sensor Systems for the Early Earth Observing System Platforms*. doi:10.1117/12.152835

Roesler, C., Uitz, J., Claustre, H., Boss, E., Xing, X., Organelli, E., et al. (2017). Recommendations for obtaining unbiased chlorophyll estimates from in situ chlorophyll fluorometers: A global analysis of WET Labs ECO sensors. *Limnology and Oceanography: Methods,15*(6), 572-585. doi:10.1002/lom3.10185

Roy, T., Rayner, P., Matear, R., & Francey, R. (2003). Southern hemisphere ocean CO2 uptake: Reconciling atmospheric and oceanic estimates. *Tellus B,55*(2), 701-710. doi:10.1034/j.1600-0889.2003.00058.x

Russell, J., Sarmiento, J., Cullen, H., Hotinski, R., Johnson, K., Riser, S., & Talley, L. (2014, Fall). The Southern Ocean Carbon and Climate Observations and Modeling Program (SOCCOM). *Ocean Biogeochemistry News*, *7*. Retrieved from https://www.us-ocb.org/wp-content/uploads/sites/43/2016/12/OCB_NEWS_FALL14.pdf

R Core Team (2017) R: A language and environment for statistical computing. R Foundation for Statistical Computing

Sabine, C. L., Feeley, R.A., Gruber, N., Key, R.M., Lee, K., Bullister, J.L., et al. (2004). The Oceanic Sink for Anthropogenic CO2. *Science,305*(5682), 367-371. doi:10.1126/science.1097403

Sackmann, B. S., Perry, M. J., & Eriksen, C. C. (2008). Seaglider observations of variability in daytime fluorescence quenching of chlorophyll-*a* in Northeastern Pacific coastal waters. *Biogeosciences Discussions,5*(4), 2839-2865. doi:10.5194/bgd-5-2839-2008

Smetacek, V., Klaas, C., Strass, V. H., Assmy, P., Montresor, M., Cisewski, B., et al. (2012). Deep carbon export from a Southern Ocean iron-fertilized diatom bloom. *Nature,487*(7407), 313-319. doi:10.1038/nature11229

Soppa, M., Dinter, T., Taylor, B., & Bracher, A. (2013). Satellite derived euphotic depth in the Southern Ocean: Implications for primary production modelling. *Remote Sensing of Environment,137*, 198-211. doi:10.1016/j.rse.2013.06.017

Strutton, P. G., Martz, T. R., Degrandpre, M. D., Mcgillis, W. R., Drennan, W. M., & Boss, E. (2011). Bio-optical observations of the 2004 Labrador Sea phytoplankton bloom. *Journal of Geophysical Research,116*(C11). doi:10.1029/2010jc006872

Sverdrup, H. U. (1953). On Conditions for the Vernal Blooming of Phytoplankton. *ICES Journal of Marine Science,18*(3), 287-295. doi:10.1093/icesjms/18.3.287

Takahashi, T., Sutherland, S. C., Sweeney, C., Poisson, A., Metzl, N., Tilbrook, B., et al. (2002). Global sea–air CO2 flux based on climatological surface ocean pCO2, and seasonal biological and temperature effects. *Deep Sea Research Part II: Topical Studies in Oceanography,49*(9-10), 1601-1622. doi:10.1016/s0967-0645(02)00003-6

Tagliabue, A., Aumont, O., & Bopp, L. (2014). The impact of different external sources of iron on the global carbon cycle. *Geophysical Research Letters,41*(3), 920-926. doi:10.1002/2013gl059059

Thomalla, S. J., Fauchereau, N., Swart, S., & Monteiro, P. M. (2011). Regional scale characteristics of the seasonal cycle of chlorophyll in the Southern Ocean. *Biogeosciences Discussions,8*(3), 4763-4804. doi:10.5194/bgd-8-4763-2011

Webb Research, T. (2012), *APEX Profiler User Manual*, Teledyne Webb Research, A Teledyne Instruments, Inc. Company, 82 Technology Park Drive, E. Falmouth Massachusetts 02536.

Xing, X., Claustre, H., Blain, S., Dortenzio, F., Antoine, D., Ras, J., et al. (2012). Quenching correction for in vivo chlorophyll fluorescence acquired by autonomous platforms: A case study with instrumented elephant seals in the Kerguelen region (Southern Ocean). *Limnology and Oceanography: Methods,10*(7), 483-495. doi:10.4319/lom.2012.10.483